nature communications

Article

https://doi.org/10.1038/s41467-026-71917-8

An anti-adhesive compound modulating the production of *Staphylococcus aureus* cell wall-anchored proteins

Received: 14 March 2025

Accepted: 2 April 2026

Published online: 15 April 2026

Check for updates

Allison C. Leonard[1], Ruina Bao[1], Cindy Menjivar[2], Megan J. Myers[2], Telmo O. Paiva[3], Zhiyong Zheng[3], Kirsten A. Berry[1], Kenneth W. Bayles[4], Ronald S. Flannagan[5], Yves F. Dufrêne[3], Jeffrey L. Bose[2], David E. Heinrichs[5] & Georgina Cox[1]

As one of the leading global causes of death associated with antimicrobial resistance, *Staphylococcus aureus* frequently colonizes the human nasal cavity and adheres to keratinized skin, establishing reservoirs that drive subsequent infections and emphasize the need for new decolonization strategies. Using a high-throughput, whole-cell screening platform, here we identify geranylgeranoic acid (GGA), a naturally occurring polyunsaturated, branched-chain fatty acid, as having dual activity against methicillin-resistant *S. aureus* (MRSA). At elevated concentrations, GGA exhibits microbicidal effects, whereas at sub-microbicidal doses, it effectively inhibits MRSA adhesion to keratin, fibronectin, fibrinogen, and immunoglobulins. GGA possesses anti-adhesive activity against a panel of multidrug-resistant *S. aureus* clinical isolates and demonstrates efficacy against MRSA skin and soft tissue infections in mice, offering a promising new avenue for combating this challenging pathogen. The anti-adhesive activity of GGA is attributed to the transcriptional modulation of *S. aureus* cell wall-anchored (CWA) proteins. For the fibronectin-binding proteins, this effect is mediated by inhibition of the SaeRS two-component system, which, in turn, down-regulates a variety of *S. aureus* virulence determinants. Our data also suggest that GGA targets additional transcriptional regulators beyond SaeRS. These insights expand the translational relevance of our findings and underscore the potential of GGA as an anti-MRSA therapeutic.

S taphylococcus aureus is the leading global contributor to deaths both associated with and attributable to antimicrobial resistance[1]. The organism is a major cause of infections in both community and hospital settings, driven by its ability to colonize human skin, with over 80% of the adult population being intermittently colonized and ~20% persistently colonized in the anterior nasal cavity[2,3]. Underscoring the ability of *S. aureus* to colonize the nasal epithelium is the production of cell wall-anchored (CWA) adhesins such as clumping factor B (ClfB) that strongly bind to host cornified envelope proteins in the epidermis, including keratin and loricrin, preventing clearance by host defense mechanisms[3–7]. Following colonization, additional CWA proteins and other virulence determinants play a pivotal role in establishing

[1]College of Biological Sciences, Department of Molecular and Cellular Biology, University of Guelph, 50 Stone Rd E, Guelph, ON, Canada. [2]Department of Microbiology, Molecular Genetics and Immunology, University of Kansas Medical Center, Kansas City, KS, USA. [3]Louvain Institute of Biomolecular Science and Technology, UCLouvain, Croix du Sud, 4-5, bte L7.07.07, B-1348, Louvain-la-Neuve, Belgium. [4]Department of Pathology and Microbiology. University of Nebraska Medical Center, Omaha, NE, USA. [5]Department of Microbiology and Immunology, University of Western Ontario, London, Ontario, Canada. e-mail: gcox@uoguelph.ca

infections through interactions with host ligands, thereby driving disease progression[7]. Most *S. aureus* infections arise from these colonizing strains, highlighting the critical role of host adhesion and the potential for therapeutics targeting this process[3,8,9]. While preoperative nasal decolonization with the antibiotic mupirocin is routine[10], resistance is increasing, with rates reported as high as 80%[11]. New and alternative decolonization strategies are urgently needed, particularly those that do not favour the evolution of resistance by avoiding essential growth pathways.

Anti-adhesives hold promise for addressing this growing clinical need; however, only a few examples of such inhibitors exist for *S. aureus*[3,12], and no clinically approved agents are available, highlighting the need for further exploration of this therapeutic approach. Identifying inhibitors of *S. aureus* adhesion has been challenging due to the limited availability of high-throughput, whole-cell assays for chemical screens[13]. Traditional methods often focus on specific targets (e.g., the housekeeping transpeptidase sortase A, responsible for covalently anchoring adhesins to the cell wall[14]), which restricts discovery to a narrow range of potential inhibitors. In contrast, a whole-cell assay allows for an unbiased, phenotypic screen that can sample a much broader target space and identify compounds with diverse mechanisms of action. Crucially, cell-based assays ensure the biological activity of identified inhibitors, a frequent limitation in target-based drug discovery[15,16]. To overcome this bottleneck, we developed a novel ELISA-based high-throughput whole-cell assay to detect *S. aureus* adhesion to host ligands[13].

Harnessing this assay to identify anti-adhesive compounds, we report the identification of geranylgeranoic acid (GGA) as an inhibitor of transcriptional regulators controlling the production of CWA adhesive proteins and other *S. aureus* virulence factors. GGA disrupts *S. aureus* adhesion to key host ligands—keratin, fibronectin, fibrinogen, and immunoglobulins—and exhibits anti-adhesive activity against clinical isolates. Efficacy in a mouse model of skin infection highlights its potential as an anti-MRSA agent. Our results also further emphasize the multifaceted role of unsaturated fatty acids within the innate immune response.

Results

Identification of geranylgeranoic acid (GGA) as an inhibitor of *S. aureus* adhesion to keratin

Given the critical role of *S. aureus* keratin adhesion in host colonization and infection[3], we sought to identify inhibitors of this process by adapting our ELISA-based MRSA adhesion assay for high-throughput chemical screening (Fig. 1A)[13]. We screened a library of 3,921 bioactive compounds (Supplementary Data 1) against the CA-MRSA strain JE2, derived from the USA300 clone—the dominant MRSA lineage in North America[17–19]. The bioactive compound collection includes FDA-approved drugs, purified natural products, and structurally diverse molecules with drug-like properties. The JE2 strain was propagated in the presence of each compound until an OD_{600nm} of 0.6 was achieved, representing optimal keratin adhesion[13]. The treated cells were then applied to microtiter plates coated with keratin, and adhesion was measured. The ratio between adhesion (Abs_{450nm}) and growth (OD_{600nm}) for each compound was determined, and the data were normalized by the mean of the middle 50% of ordered values, known as the interquartile mean (IQM)[20]. A hit was defined as a ratio of <0.75 (Fig. 1B), selecting for compounds that did not inhibit growth by >25% at 10 µM (Fig. 1C) while reducing adhesion by ≥30% (Fig. 1D). This screen resulted in a hit rate of 0.3% and highlighted the enrichment of amphipathic compounds (Table S1).

To confirm their anti-adhesive properties, the potency and reproducibility of each hit were assessed, identifying geranylgeranoic acid (GGA) as a lead compound (Fig. 1A). GGA is a naturally occurring diterpenoid that resembles a polyunsaturated, branched-chain fatty acid naturally occurring in medicinal plants[21]. It is a precursor to geranylgeranyl pyrophosphate, an essential intermediate in the biosynthesis of isoprenoids. GGA exhibits cancer-preventative activity[22] and moderate to weak antibacterial activity against several bacterial species, including *Salmonella typhimurium*, *Proteus vulgaris*, *Bacillus subtilis*, and *Escherichia coli*[23].

GGA was resupplied, and dose-dependent analyses using the ELISA-based adhesion assay confirmed that GGA inhibits keratin adhesion at sub-growth-inhibitory concentrations (Fig. 1E). Scanning

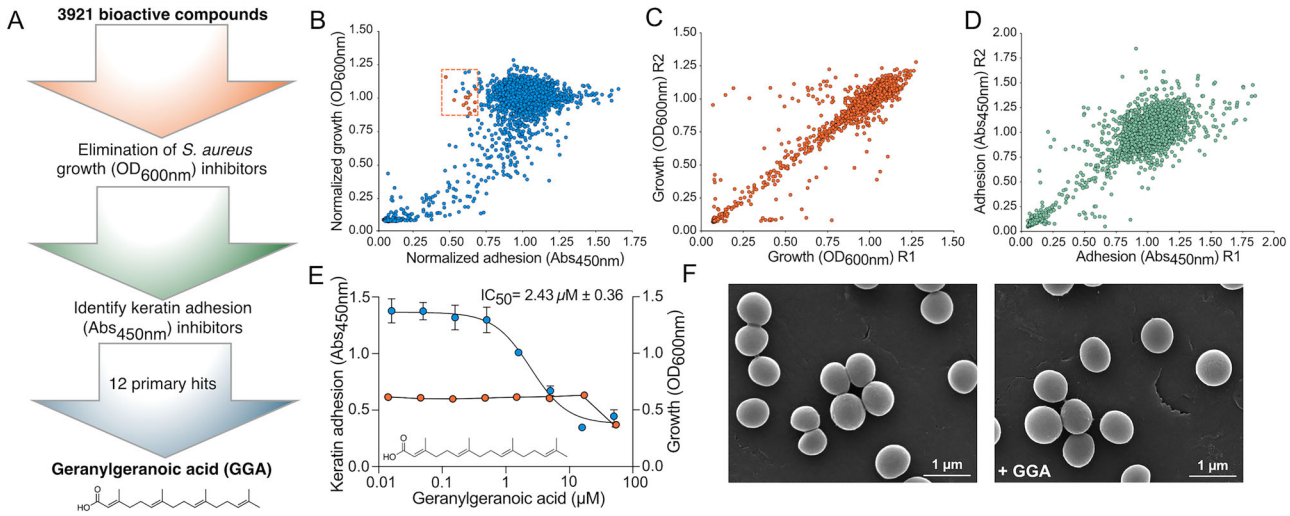

Fig. 1 | Identification of geranylgeranoic acid (GGA) as an inhibitor of methicillin-resistant *S. aureus* (MRSA) adhesion to human keratin. A The workflow undertaken in the high-throughput chemical screen. **B** Large-scale profiling of the bioactive compound collection ($n = 3921$) against the MRSA USA300 strain JE2 (JE2). A hit was defined as a compound that reduced adhesion by ≥30% (Abs_{450nm}) without impacting growth (≤25% growth inhibition) (OD_{600nm}). Hits are highlighted in the orange box. **C** Replica plot of keratin adhesion (Abs_{450nm}) and (**D**) bacterial growth (OD_{600nm}) in the presence of each compound. R1 = biological replicate one, and R2 = biological replicate two. **E** Dose titration adhesion assay (blue circles, Abs_{450nm}) and growth inhibitory analysis (orange circles, OD_{600nm}) of JE2 cells treated with GGA. The GGA chemical structure and half-maximal inhibitory concentration of adhesion (mean Adhesion IC_{50} ± the standard error, $n = 3$ biological replicates) are shown. Each orange data point represents the mean growth of $n = 3$ biological replicates, and the error bars represent the standard deviation (SD). **F** Scanning electron microscopy analysis of JE2 cells (0.05% ethanol) ± GGA (10 µM in 0.05% ethanol). Further biological replicates ($n = 3$ biological replicates in total) are shown in Fig. S1. Source data are provided as a Source Data file.

https://doi.org/10.1038/s41467-026-71917-8

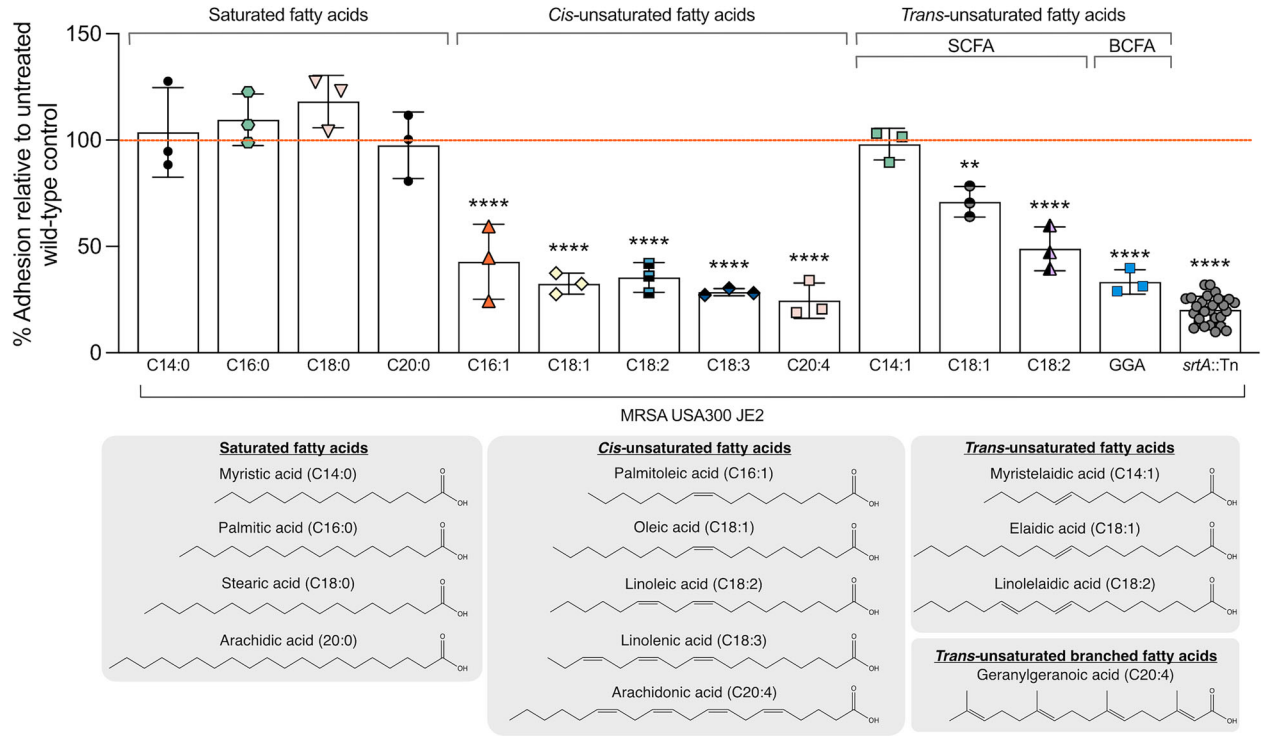

Fig. 2 | GGA structure-activity relationship studies. Structure-activity relationships were assessed by evaluating the inhibition of MRSA USA300 JE2 (JE2) adhesion to 0.5 μg/well keratin (Abs_{450nm}) following treatment with 10 μM of saturated, *cis*-unsaturated, and *trans*-unsaturated fatty acids. GGA (10 μM, blue squares) is included for comparison. The chemical structures of each fatty acid are shown in the grey boxes. Adhesion was measured for JE2 treated with each fatty acid in independent experiments ($n = 3$ biological replicates per experiment). Each data point corresponds to a single biological replicate, with the mean and standard deviation (SD) shown. Fatty acid-treated samples were normalized to the untreated control (JE2) included in each independent experiment, as represented by the orange line. The JE2-*srtA*::Tn untreated mutant was included as an adhesion-defective control when profiling each fatty acid. Fatty acid-treated samples and the JE2-*srtA*::Tn mutant were compared to JE2 (100%) using a two-tailed, one-sample *t*-test. Statistically significant decreases in adhesion compared to the untreated control (JE2) are denoted as $P \leq 0.01$**, and $P \leq 0.0001$****. Related to Figs. S3 and S4. SCFA: straight-chain fatty acid; BCFA: branched-chain fatty acid. Exact *P* values (versus JE2): C14:0, $P = 0.780$; C14:1, $P = 0.684$; C16:0, $P = 0.242$; C16:1, $P = 0.005$; C18, $P = 0.063$; C18:1(cis), $P = 1.9E\text{-}05$; C18:1(trans), $P = 0.002$; C18:2(cis), $P = 8.9E\text{-}05$; C18:2(trans), $P = 0.001$; C18:3, $P = 1.9E\text{-}07$; C20, $P = 0.800$; C20:4, $P = 9.7E\text{-}05$; GGA, $P = 3.6E\text{-}05$; and *srtA*::Tn, $P \leq 0.0001$. Source data are provided as a Source Data file.

electron micrography analysis demonstrated that GGA does not impact the morphology of *S. aureus* compared to the untreated control (Fig. 1F and Fig. S1). The anti-adhesive properties of GGA were further confirmed using crystal violet as an alternative detection method (Fig. S2A). Finally, the anti-adhesive activity of the compound was observed to be pH-dependent, with increased potency within a pH range of 7–9 (Fig. S2B). In these assays, an adhesion-defective transposon (Tn) mutant control strain (*srtA*::Tn) was included that lacked the housekeeping sortase, sortase A (SrtA), responsible for covalently anchoring *S. aureus* adhesive proteins to the peptidoglycan[14]. GGA treatment inhibited adhesion to the level of the *srtA*::Tn mutant, demonstrating that the compound is a potent anti-adhesive (Fig. S2B). Due to the pH-associated relationship of GGA (Fig. S2B), all subsequent mechanistic experiments were performed with cells propagated in growth medium buffered at pH 7.0, corresponding to optimal GGA activity.

GGA structure-activity relationship studies

To better understand the chemical features of GGA associated with anti-adhesive activity, we undertook a structure-activity relationship (SAR) study. We began by performing an in silico analysis of the bioactive compound collection profiled during the primary screen. Such an approach revealed that the carboxylic acid moiety was important for bioactivity, as three alcohols exhibiting similar poly-unsaturation and branching to GGA—including the alcohol derivative of GGA, geranylgeraniol—lacked activity in the primary screen and were therefore eliminated at that stage.

To explore whether other fatty acids (FAs) also inhibit *S. aureus* keratin adhesion, we selected a panel with different chain lengths and saturation levels (Table S2). We first assessed their growth inhibitory effects, revealing varying degrees of inhibition (Table S2). The anti-adhesive activity of each FA was then assessed at 10 μM (Fig. 2 & Table S2), a concentration that was sub-inhibitory for growth (Fig. S3). Overall, we found that saturated FAs did not exhibit anti-adhesive activity, yet all the *cis*-unsaturated FAs and two *trans*-unsaturated FAs inhibited keratin adhesion. *Cis*-unsaturated FAs demonstrated greater anti-adhesive potency than trans-unsaturated FAs (Fig. 2). Specifically, *cis*-FAs with a kinked carbon chain exhibited anti-adhesive activity comparable to that of geranylgeranoic acid (GGA) and the adhesion-defective *srtA*::Tn mutant (Fig. 2). To ensure comprehensive analysis, FAs lacking initial anti-adhesive activity were tested at higher concentrations (Fig. S4 and Table S2), remaining below levels that visibly affected bacterial growth (Fig. S3) and ensuring solubility (Table S2). Myristic acid (C14:0) showed weak anti-adhesive activity at 100 μM, whereas myristelaidic acid (trans-C14:1) displayed similar potency to GGA at 50 μM. The remaining FAs did not exhibit anti-adhesive activity even at these elevated concentrations (Fig. S4). Our results indicate that the presence of a *cis* double bond is crucial for anti-adhesive activity; chain length does not appear to be a significant factor. While increased chain length correlates with anti-adhesive activity when the double bond is in the *trans* configuration, the overall potency remains lower. Therefore, both the carboxylic acid moiety and degree of unsaturation are key determinants of GGA's activity. Importantly,

https://doi.org/10.1038/s41467-026-71917-8

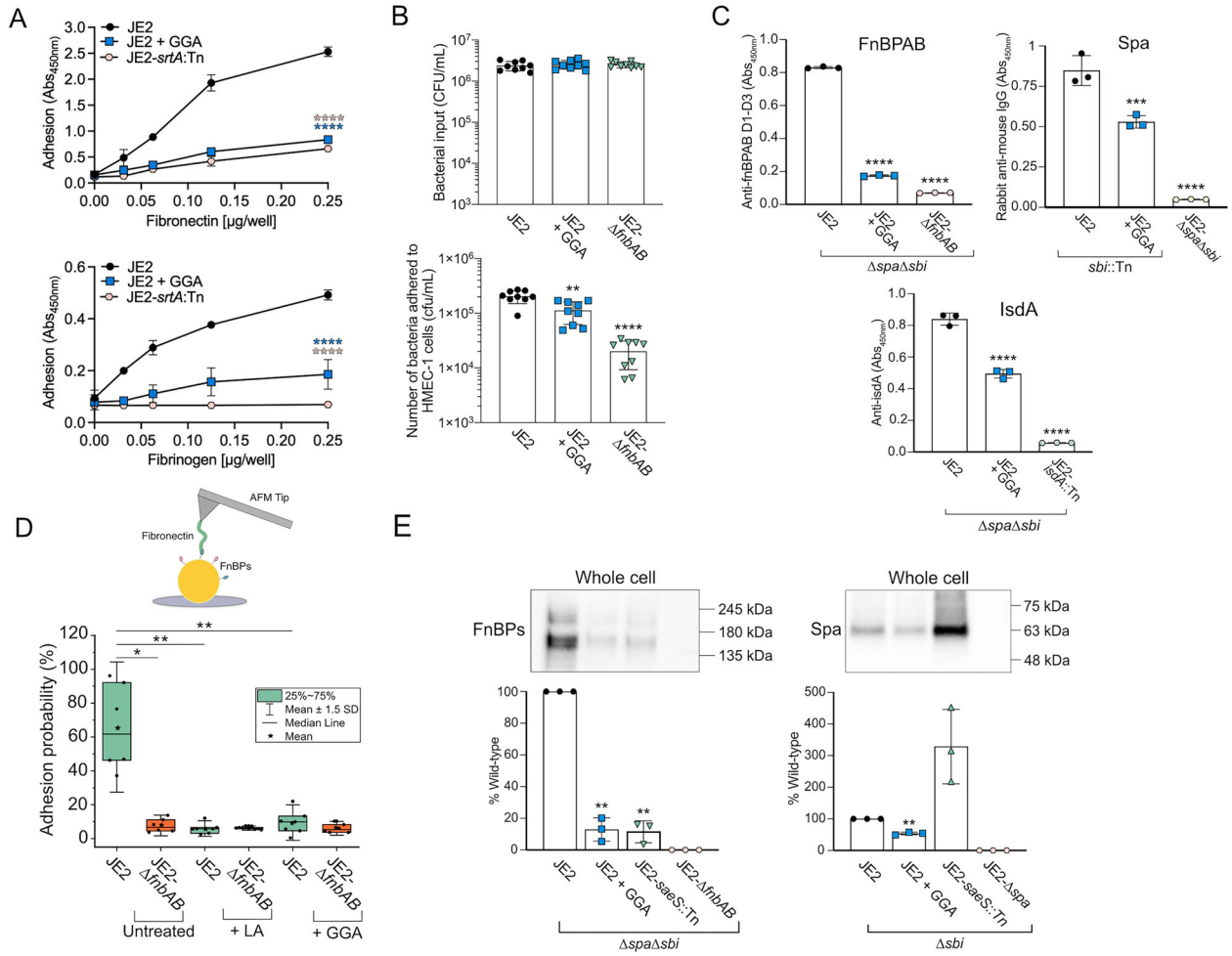

Fig. 3 | GGA is a broad-spectrum anti-adhesive modulating *S. aureus* cell wall-anchored (CWA) proteins. A Reduction in MRSA USA300 JE2 (JE2) adhesion (Abs_{450nm}) to fibronectin and fibrinogen following 10 μM GGA treatment (Related to Fig. S5A, B). Data points represent the mean of $n = 3$ biological replicates ± SD. The JE2-*srtA*::Tn mutant was included as an adhesion-defective negative control. Adhesion to fibronectin exact *P* values: JE2 + GGA (versus JE2), $P = 1.4E\text{-}05$ and JE2-*srtA*::Tn (versus JE2), $P = 9.3E\text{-}06$. Adhesion to fibrinogen exact *P* values: JE2 + GGA (versus JE2), $P = 6.0E\text{-}05$ and JE2-*srtA*::Tn (versus JE2), $P = 4.5E\text{-}06$. **B** The effect of GGA (10 μM) treatment on JE2 adhesion to HMEC-1 endothelial cells. Each data point represents a single bacterial biological replicate ± SD of the mean ($n = 9$ biological replicates). Differences were assessed using a Brown-Forsythe and Welch's ANOVA followed by Dunnett's T3 multiple comparisons test to compare each experimental group to the untreated control (JE2). $P \leq 0.01$** and $P \leq 0.0001$****. **C** GGA treatment (10 μM) reduced the abundance of the fibronectin-binding proteins (FnBPAB), Spa, and IsdA on the surface of immobilized whole JE2 cells (Fig. S5C). Each data point represents a single biological replicate ($n = 3$ biological replicates), and the error bars show the SD of the mean. For (**A**) and (**C**), differences among groups were assessed using a one-way ANOVA followed by Dunnett's multiple comparisons test to compare each experimental group to the untreated control (JE2). $P \leq 0.001$***, and $P \leq 0.0001$****. **D** Box plots showing the fibronectin adhesion probability of JE2 (green) and JE2-Δ*fnbAB* (orange) cells treated with GGA and linoleic acid (LA) (10 μM), which was assessed using AFM-based single-molecule force spectroscopy (the setup is shown). $n = 6, 6, 7, 9, 7$, and 6 cells probed for each condition (Related to Figs. S6, S7). Stars indicate mean values, lines medians, boxes 25–75% quartiles, and whiskers SD. *P*-values were calculated using a one-way Brown-Forsythe and Welch ANOVA test with a Dunnett T3 multiple comparisons test. $P < 0.05$ * and $P \leq 0.01$**. Exact *P*-values: JE2-Δ*fnbAB* (versus JE2), $P = 0.011$, JE2 + LA (versus JE2), $P = 0.0095$ and JE2 + GGA (versus JE2), $P = 0.008$. **E** Immunoblots of FnBPs and Spa from JE2 whole cell lysates were normalized to total protein using a stain-free approach (Fig. S5D). The FnBPs are shown as the cumulative intensity of FnBPA and FnBPB. Protein levels are expressed relative to the untreated control (JE2). Representative immunoblots from one replicate are shown. Data are represented as the mean ± SD of $n = 3$ biological replicates. Statistical significance of each experimental group compared to JE2 (set at 100%) was determined by a one-sample *t*-test with Bonferroni correction for multiple comparisons. $P \leq 0.01$**. Exact *P*-values for Fnbps immunoblot: JE2 + GGA (versus JE2), $P = 0.0048$ and JE2-*saeS*::Tn (versus JE2), $P = 0.0048$. Exact *P*-values for Spa immunoblot: JE2 + GGA (versus JE2), $P = 0.0054$ and JE2-*saeS*::Tn (versus JE2), $P = 0.1562$. Source data are provided as a Source Data file.

although FAs are known to impede biofilm formation[24–26], this is the first report that they also inhibit *S. aureus* adhesion to host ligands.

GGA modulates the production of *S. aureus* cell wall-anchored (CWA) proteins

Next, to gain insight into GGA's mechanism of action, we investigated whether its anti-adhesive activity was specific to keratin or also applies to other host ligands. We found that GGA treatment significantly diminished *S. aureus* binding to several host ligands, including fibronectin (Fig. 3A and S5A) and fibrinogen (Fig. 3A and S5B). Fibronectin binding enables *S. aureus* to associate with endothelial cells, triggering actin remodeling and invasion[27–31]. To test the biological relevance of our results, we evaluated how GGA treatment affected *S. aureus* adhesion to an immortalized human microvascular endothelial cell line (HMEC-1); treatment with GGA significantly reduced adhesion (Fig. 3B). Thus, our findings demonstrate that GGA not only impairs keratin adhesion but also broadly inhibits *S. aureus* adhesion, leading us to hypothesize that the compound modulates the abundance or surface localization of cell wall-anchored (CWA) proteins. These surface proteins mediate *S. aureus* binding to the diverse host ligands affected by

GGA, and are covalently attached to the peptidoglycan via sortase A (SrtA), the housekeeping transpeptidase[14,32,33]. Indeed, the finding that GGA reduced *S. aureus* adhesion to a degree comparable with the *srtA*::Tn mutant (Figs. 2 and 3A) further supports the hypothesis that GGA may be modulating CWA proteins.

To investigate this possibility, we employed an ELISA-based whole-cell approach[12] to measure the surface abundance of structurally diverse CWA proteins from different classes. The major CWA keratin adhesin in *S. aureus* is ClfB; however, attempts to measure the surface abundance of ClfB were unsuccessful since commercial anti-ClfB antibodies cross-reacted with other surface proteins, and a custom monospecific antibody from Pacific Immunology also failed to provide reliable surface detection. Because GGA reduced *S. aureus* binding to fibronectin (Fig. 3A) and since we possess an antibody against the CWA fibronectin-binding proteins (FnBPs), we sought to assess their surface abundance. In addition, to determine whether GGA broadly affects CWA proteins, we also examined two other distinct CWA proteins for which antibodies are available[12,34]: the *S. aureus* immunoglobulin-binding protein A (SpA)[35], which aids immune evasion, and iron-regulated surface determinant A (IsdA), which binds host hemoglobin and ferric–heme, facilitating iron acquisition in the host[36]. Evaluation of CWA surface abundance was performed using a USA300 strain devoid of the *S. aureus* immunoglobulin-binding protein A (SpA) and the second immunoglobulin-binding protein (Sbi), except when evaluating the impact of GGA treatment on *S. aureus* IgG binding, mediated by SpA, when only a *sbi* mutant was used (*sbi*::Tn). Whole *S. aureus* cells were immobilized on the surface of polystyrene microtiter plates (Fig. S5C), and GGA was shown to significantly reduce the surface abundance of all three CWA proteins compared to the untreated control (Fig. 3C).

To further confirm these findings, we used a more direct method to measure the surface abundance of the FnBPs, employing single-molecule force spectroscopy (SMFS) with fibronectin-functionalized atomic force microscopy (AFM) tips (Fig. 3D) to force probe individual *S. aureus* whole live cells treated with GGA or linoleic acid, another unsaturated fatty acid with anti-adhesive properties (Fig. 2). SMFS confirmed that the untreated cells exhibit FnBP-mediated adhesion to fibronectin (Fig. 3D), characterized by strong forces (Fig. S6A), typical of this interaction[37]. By contrast, consistent with previous literature, we observed a near complete loss of adhesion in a mutant devoid of the FnBPs (MRSA USA300 JE2 Δ*fnbAB*), which confirmed that these interactions were FnBP-mediated (Fig. 3D and S7)[37,38]. Overall, GGA and linoleic acid-treated cells had significantly fewer interactions and exhibited adhesion forces comparable to cells devoid of the FnBPs (Fig. 3D & S7). SMFS also allowed spatial mapping of protein distribution on the cell surface (Figs. S6 and S7), revealing the presence of adhesion nanodomains, which we attribute to clustering on the cell surface, a mechanism used by bacteria to enhance adhesion[39]. Finally, to determine whether GGA affected the overall cellular abundance of CWA proteins or specifically disrupted their surface display, immunoblotting was performed to assess FnBP and SpA levels in whole-cell lysates (Fig. 3E). GGA treatment reduced the overall cellular abundance of both proteins (Fig. 3E).

The anti-adhesive activity of GGA is independent of protease production in *S. aureus*

Post-translational degradation by proteases may affect the cellular abundance of CWA surface proteins in *S. aureus*[40]. We initially hypothesized that GGA activates the Staphylococcal Proteolytic Cascade (SPC)[41], which includes aureolysin, SspA, and SspB. These proteases cleave both bacterial and host proteins, including many CWA proteins, thereby affecting their stability and potentially reducing adhesion[42–47]. We investigated the effect of GGA on protease production by profiling the abundance of glycerol ester hydrolase (Geh), a secreted lipase susceptible to proteolysis[48,49]. FAs such as linoleic acid induce the SPC, increasing cleavage of the 72-kDa Geh precursor isoform (pro-Geh) into mature 40-kDa Geh, detectable by SDS-PAGE analysis of secreted proteins[41]. Treatment with GGA, or the control fatty acid linoleic acid[41], both increased Pro-Geh cleavage in MRSA USA300 strain AH1263 cells compared to the untreated control (Fig. 4A and S8). A protease-null mutant (KB4058 Δ*aur*; *sspA; sspB; scpA*, *htrA1*, *htrA2, splABCDEF*::Eryr) served as a negative control because it cannot process pro-Geh into its mature form. However, while GGA increased protease production, we also demonstrated that GGA inhibited adhesion of the protease-null KB4058 mutant (Fig. 4B), highlighting that the mechanism of action is distinct from protease induction.

GGA is not incorporated into the *S. aureus* membrane phospholipids

S. aureus imports exogenous unsaturated FAs via the FA kinase (Fak) complex to complement endogenous biosynthesis[50,51]. Given that other FAs used in this study are incorporated into membrane phospholipids via Fak[50,52,53], we sought to establish whether GGA undergoes similar incorporation. We first investigated whether the Fak complex, which activates and incorporates host FAs into bacterial membranes[50,51,54], recognizes GGA as a substrate. Kinase activity was absent with GGA but robust with oleic acid, a known Fak substrate[54] (Fig. 4C). We also extracted phospholipids from GGA-treated cells and analyzed them using liquid chromatography-tandem mass spectrometry (Supplementary Data 2 & Fig. 4D). Because lysophosphatidylglycerol and cardiolipin are derived from phosphatidylglycerol, the most abundant phospholipid in *S. aureus* membranes[52], we analyzed only phosphatidylglycerol. Lipid profiles showed no significant differences between GGA-treated cells, and unsaturated FA species were absent (Supplementary Data 2 & Fig. 4D).

GGA inhibits the SaeRS two-component system

We subsequently posited that GGA was inhibiting the transcriptional regulators controlling CWA protein abundance. Host-derived free FAs are known to inhibit the SaeRS two-component system, thereby affecting virulence factor production[55–59]. Unsaturated FAs exhibit greater potency than saturated FAs in Sae inhibition, with their effectiveness influenced by the degree of unsaturation and *cis*/*trans* conformation[59], which is similar to the outcomes of our SAR study (Fig. 2). SaeRS positively regulates the CWA FnBPs[60], as confirmed using immunoblotting of whole cell JE2 lysates (Fig. 3E) and by measuring the surface abundance of FnBPs in a *saeS* transposon mutant (Fig. 5A). GGA treatment did not further reduce FnBP levels in the *saeS*::Tn mutant (Fig. 5A) or when *fnbA* was overexpressed from the leaky[61] TetR-controlled $P_{xyl/tetO}$ promoter of the pALC2073 plasmid[62] (Fig. 5B); plasmidic constitutive expression bypasses SaeRS regulation and maintains active *fnbA* transcription regardless of GGA treatment. To confirm further that GGA was impacting the activity of SaeRS, a P_{coa}-*lacZ* reporter construct was used as an indicator of Sae activity[59]. GGA-mediated inhibition of SaeRS was comparable to oleic acid, which was included as a positive control[59] (Fig. 5C).

GGA inhibits other signal transduction systems in *S. aureus*

Beyond reducing FnBP abundance through SaeRS inhibition, GGA also disrupts keratin adhesion (Fig. 1) and decreases SpA and IsdA levels (Fig. 3C). *S. aureus* adhesion to keratin and regulation of the CWA proteins, ClfB, SpA, and IsdA, have not previously been linked to SaeRS[60,63]. This prompted us to investigate how fatty acids influence these phenomena and whether the effects are transcriptional. Initially, we examined the mechanism by which GGA inhibits keratin adhesion—a process primarily mediated by ClfB, the major cell wall-anchored keratin adhesin in *S. aureus*[4,6]. We observed that GGA treatment reduced *clfB* transcript levels (Fig. S9); however, the deletion of *saeRS* did not alter *clfB* abundance (Fig. S9) or impair keratin adhesion (Fig. 5D). Additionally, the anti-adhesive activity of GGA against keratin

https://doi.org/10.1038/s41467-026-71917-8

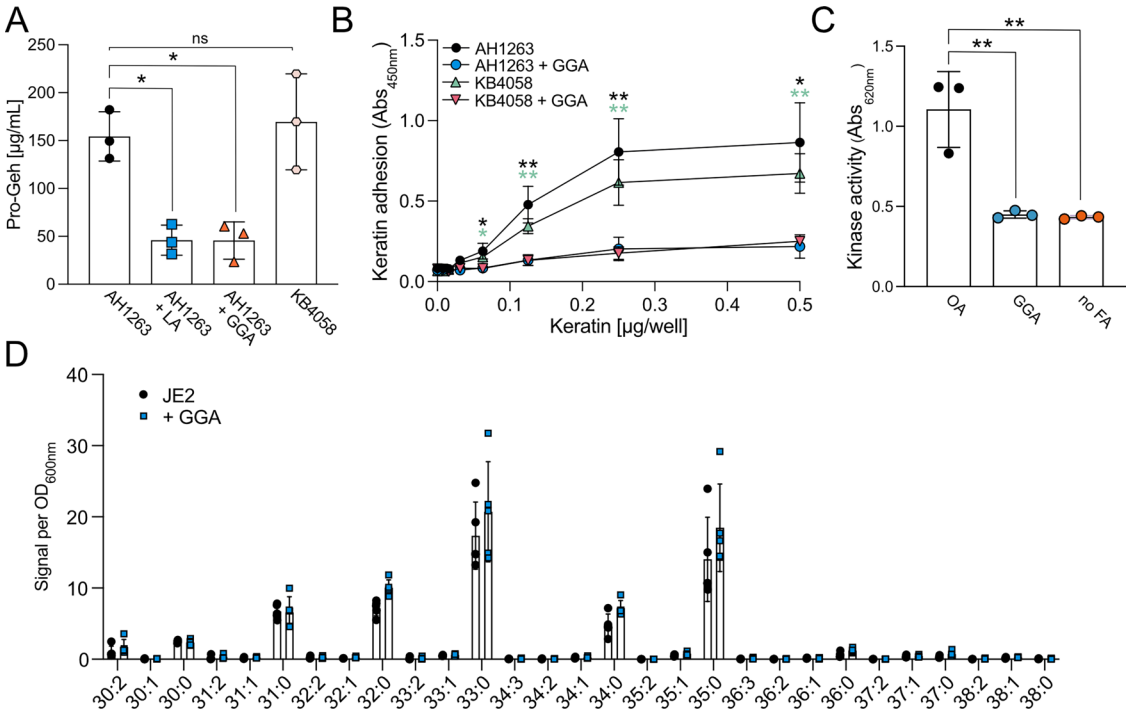

Fig. 4 | The anti-adhesive activity of GGA is not linked to protease production or membrane phospholipid incorporation. A Quantification of total pro-Geh (uncleaved Geh) in the MRSA USA300 strain AH1263 following fatty acid treatment. Each data point represents one biological replicate ($n = 3$ biological replicates in total), and the error bars represent the SD of the mean. Differences among groups were assessed using a one-way ANOVA followed by Dunnett's multiple comparisons test to compare each experimental group to the wildtype control (AH1263), $P \leq 0.01$**. Exact P values: AH1263 + LA (versus AH1263), $P = 0.0065$, AH1263 + GGA (versus AH1263), $P = 0.0067$ and KB4058 (versus AH1263), $P = 0.8772$). Related to Fig. S8. **B** ELISA-based keratin adhesion assay of AH1263 ± 10 μM GGA compared to the protease-deficient KB4058 strain ± 10 μM GGA. Each data point represents the mean of $n = 3$ biological replicates, and the error bars represent the SD of the mean. P-values were calculated using the two-tailed unpaired Student's t-test. Statistically significant decreases in surface abundance following GGA treatment compared with wild-type AH1263 or protease-null KB4058 were denoted as $P < 0.05$* and $P \leq 0.01$**, respectively. Exact P-values: AH1263 + GGA (versus AH1263), 0.5 μg/well: $P = 0.012$, 0.25 μg/well: $P = 0.009$, 0.125 μg/well: $P = 0.007$ and 0.0625 μg/well: $P = 0.023$. Exact P-values: KB4058 + GGA (versus KB4058), 0.5 μg/well: $P = 0.004$, 0.25 μg/well: $P = 0.007$, 0.125 μg/well: $P = 0.003$ and 0.0625 μg/well: $P = 0.014$. **C** In vitro activity assay for the fatty acid kinase (fak) complex in the presence of 5 mM oleic acid (OA) (positive control), 5 mM GGA, and no fatty acid. Bars represent the mean ($n = 3$ enzymatic reactions), with error bars indicating SEM. The data shown are from a representative experiment. **$P < 0.01$, as determined by one-way ANOVA followed by Dunnett's multiple comparisons test to compare each experimental group to the positive control, OA. Exact P-values OA (versus GGA), $P = 0.0020$ and OA (versus no FA), $P = 0.0018$. **D** Phosphatidylglycerol lipid profile of JE2 ± 10 μM GGA. Data are presented as the signal of each lipid species normalized to the OD_{600nm} of the culture. Each data point represents a single biological replicate ($n = 5$), and the error bars represent the SD of the mean. P-values were calculated using multiple unpaired t-tests with Holm-Šidák correction comparing GGA treatment to the untreated strain. No significant differences were detected. Exact P-values: 30:0 ($P = 0.999$), 31:0 ($P = 1.000$), 32:0 ($P = 0.090$), 33:0 ($P = 0.999$), 34:0 ($P = 0.419$) and 35:0 ($P = 0.996$). Source data are provided as a Source Data file.

remains effective even in a *saeS*::Tn mutant (Fig. 5D), and GGA treatment reduced *clfB* transcript levels in the *saeS*::Tn mutant (Fig. S9). Together, these data demonstrate that GGA treatment reduces *clfB* transcript levels, thereby reducing the affinity of *S. aureus* for keratin, which is not associated with the SaeRS system.

Consistent with this finding, the *saeS*::Tn mutant exhibited increased surface SpA levels while IsdA remained unchanged; GGA treatment still diminished both CWA proteins in this strain (Fig. 5E). While the measurement of *spa* transcript levels in response to *saeRS* disruption and GGA treatment were inconclusive due to high variability (Fig. S9), the overexpression of *spa* using the pALC2073 plasmid, which circumvents transcriptional regulation, abolished the effect of GGA on SpA surface levels (Fig. 5F). These results indicate that GGA likely inhibits other transcriptional regulators in addition to SaeRS (Fig. 5G).

We then performed a transcriptomic time-course study to compare *S. aureus* responses to *saeS* disruption (*saeS*::Tn) with those induced by GGA treatment (Fig. 6). A time-course approach was chosen because virulence gene expression varies throughout the bacterial growth cycle; this allowed us to capture a complete picture of how GGA affects *S. aureus* virulence pathways. Genes downregulated after *saeS* disruption were consistent with previous studies[63] and encompassed key virulence factors—hemolysins, adhesins, proteases, phospholipases, and leukocidins—such as *fnbA, fnbB, hla, sbi, lukH*, and *lukG* (Fig. 6 and Supplementary Data 3). GGA treatment largely reproduced the *saeS*::Tn mutant phenotype (Fig. 6A, B), confirming its ability to disrupt this two-component system. However, GGA also induced distinct transcriptional changes that point to additional cellular pathways and targets affected by the compound (Fig. 6B). Consistent with our earlier observation (Fig. 5D and Fig. S9) that *saeRS* does not regulate *clfB* (the gene encoding the main cell-wall-anchored keratin adhesin), we found that at an OD_{600nm} of 0.6, the optimal phase for keratin adhesion[13], GGA treatment reduced *clfB* expression by over fivefold (Fig. 6, Supplementary Data 3). In contrast, the *saeRS* mutant showed no change in *clfB* transcription. Moreover, GGA suppressed additional virulence-associated genes that remained unchanged upon *saeS* disruption (Fig. 6, Supplementary Data 3). These included genes encoding adhesins (*spa* and *clfB*), phenol-soluble modulins, genes involved in purine and pyrimidine biosynthesis (*pyrF/E, purA/P/R/B*), and efflux pumps (*norB*). Additionally, consistent with previous studies investigating global *S. aureus* transcriptional changes in response to 10 μM linoleic acid, we observed stimulation of the type VII secretion system and urease genes (Fig. 6, and Supplementary Data 3)[64]. Notably, *farE*, encoding the FarE fatty acid efflux pump[65], was the most upregulated

https://doi.org/10.1038/s41467-026-71917-8

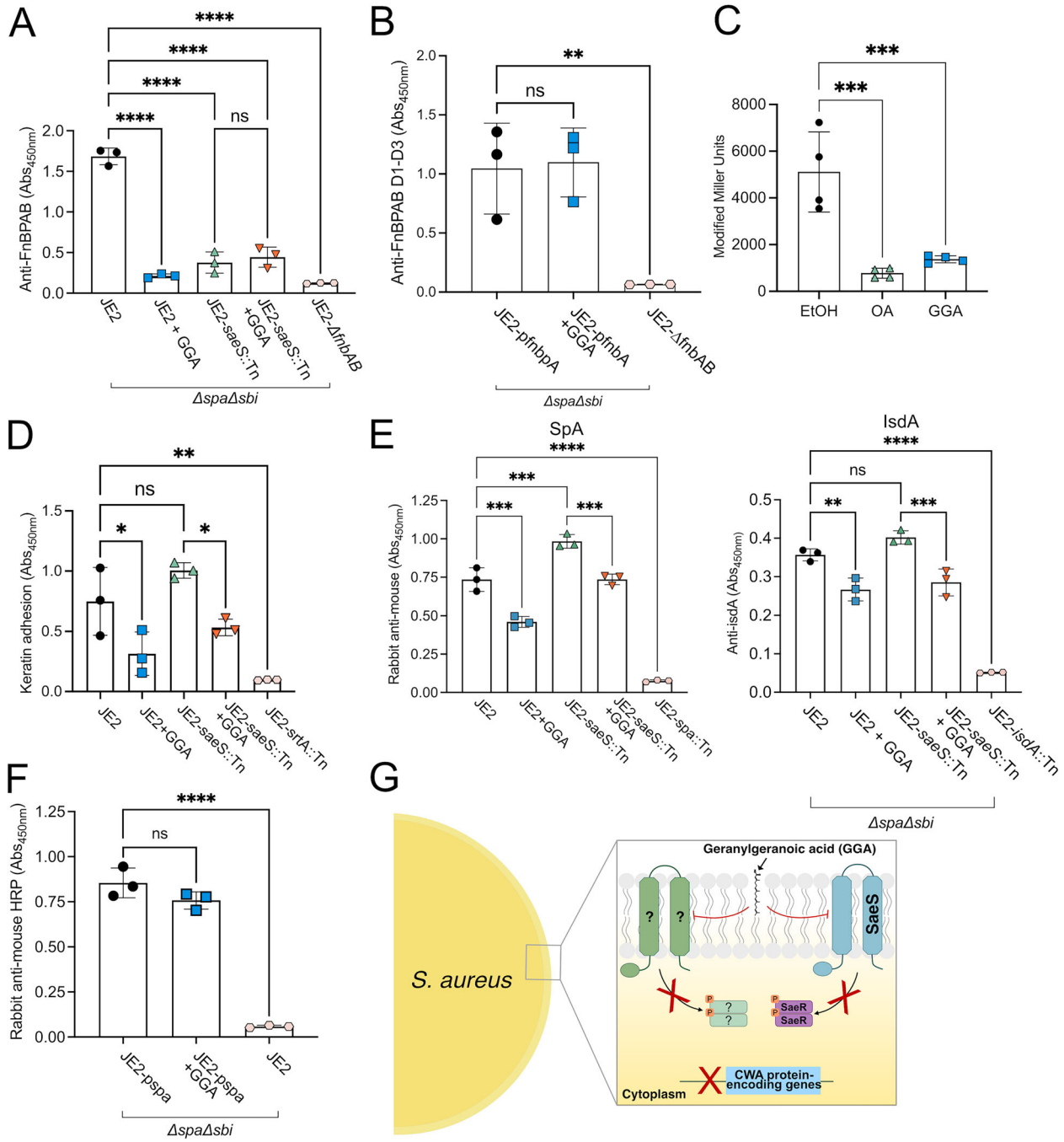

Fig. 5 | GGA inhibits SaeRS and other transcriptional regulators responsible for controlling *S. aureus* cell wall-anchored proteins. Fibronectin-binding protein (FnBPAB) abundance on the surface of (**A**) MRSA USA300 JE2 (JE2)-Δ*spa*Δ*sbi* cells and JE2-*saeS*::Tn Δ*spa*Δ*sbi* cells ± 10 μM GGA treatment, and (**B**) JE2-Δ*spa*Δ*sbi* ± 10 μM GGA when *fnbA* is expressed on a plasmid (pALC2073:*fnbA*). JE2-Δ*fnbAB* was included as a negative control. 3 biological replicates were performed per group for A through F. Data are presented as mean values +/- SD. *P*-values were calculated using a one-way ANOVA with Tukey's multiple comparisons test, $P \leq 0.01$**, $P \leq 0.0001$**** and ns= not significant. **C** Measuring the impact of GGA on SaeRS activity. P*coa-lacZ* activity of MRSA USA300 AH1263 ± 10 μM of GGA. Oleic acid (OA) (31.4 μM) was included as a positive control. *P*-values were calculated using a one-way ANOVA with Dunnett's multiple comparisons test, $P \leq 0.001$***. **D** ELISA-based keratin (0.5 μg/well) adhesion assay of JE2 and JE2-*saeS*::Tn ± 10 μM GGA. JE2-*srtA*::Tn was included as a negative control. Related to Fig. S9. *P*-values were calculated using a one-way ANOVA with Tukey's multiple comparisons test. Exact *P* values: JE2 + GGA (versus JE2), $P = 0.040$, JE2-*srtA*::Tn (versus JE2), $P = 0.003$, JE2-*saeS*::Tn (versus JE2), $P = 0.326$, and JE2-*saeS*::Tn +GGA (versus JE2-*saeS*::Tn), $P = 0.326$. **E** Spa and IsdA abundance on the surface of immobilized JE2 and JE2-*saeS*::Tn ± 10 μM GGA, and respective negative controls JE2-*spa*::Tn, and JE2-*isdA*::Tn. *P*-values were calculated using a one-way ANOVA with Tukey's multiple comparisons test. Mutants lacking the respective cell wall-anchored proteins were used as negative controls. Exact *P* values in the Spa ELISA: JE2 + GGA (versus JE2): $P = 0.0002$, JE2-*saeS*::Tn (versus JE2), $P = 0.0004$, JE2-*spa*::Tn (versus JE2), $P < 0.0001$ and JE2-*saeS*::Tn+GGA (versus JE2-*saeS*::Tn) $P = 0.0004$. Exact *P* values in the IsdA ELISA: JE2 + GGA (versus JE2), $P = 0.0052$, JE2-*isdA*::Tn (versus JE2), $P < 0.0001$, and JE2-*saeS*::Tn+GGA (versus JE2-*saeS*::Tn), $P = 0.0007$. **F** The abundance of SpA on the surface of JE2-Δ*spa*Δ*sbi* cells ± 10 μM GGA when *spa* is expressed on a plasmid (pALC2073:*spa*). Each data point represents a single biological replicate, and the error bars represent the SD of the mean. *P*-values were calculated using a one-way ANOVA with Dunnett's multiple comparisons test, comparing each strain to the wild-type strain. $P \leq 0.05$*, $P \leq 0.01$**, $P \leq 0.001$***, and $P \leq 0.0001$****. ns not significant. Exact *P* values: JE2ΔspaΔsbi-p_{spa} + GGA (versus JE2$\Delta_{spa\Delta}$sbi-p_{spa}), $P = 0.123$ and JE2$\Delta_{spa}\Delta$sbi (versus JE2-p_{spa}), $P < 0.0001$. **G** Schematic of GGA-mediated inhibition of *S. aureus* transcriptional regulators, reducing adhesion to host ligands. Source data are provided as a Source Data file.

https://doi.org/10.1038/s41467-026-71917-8

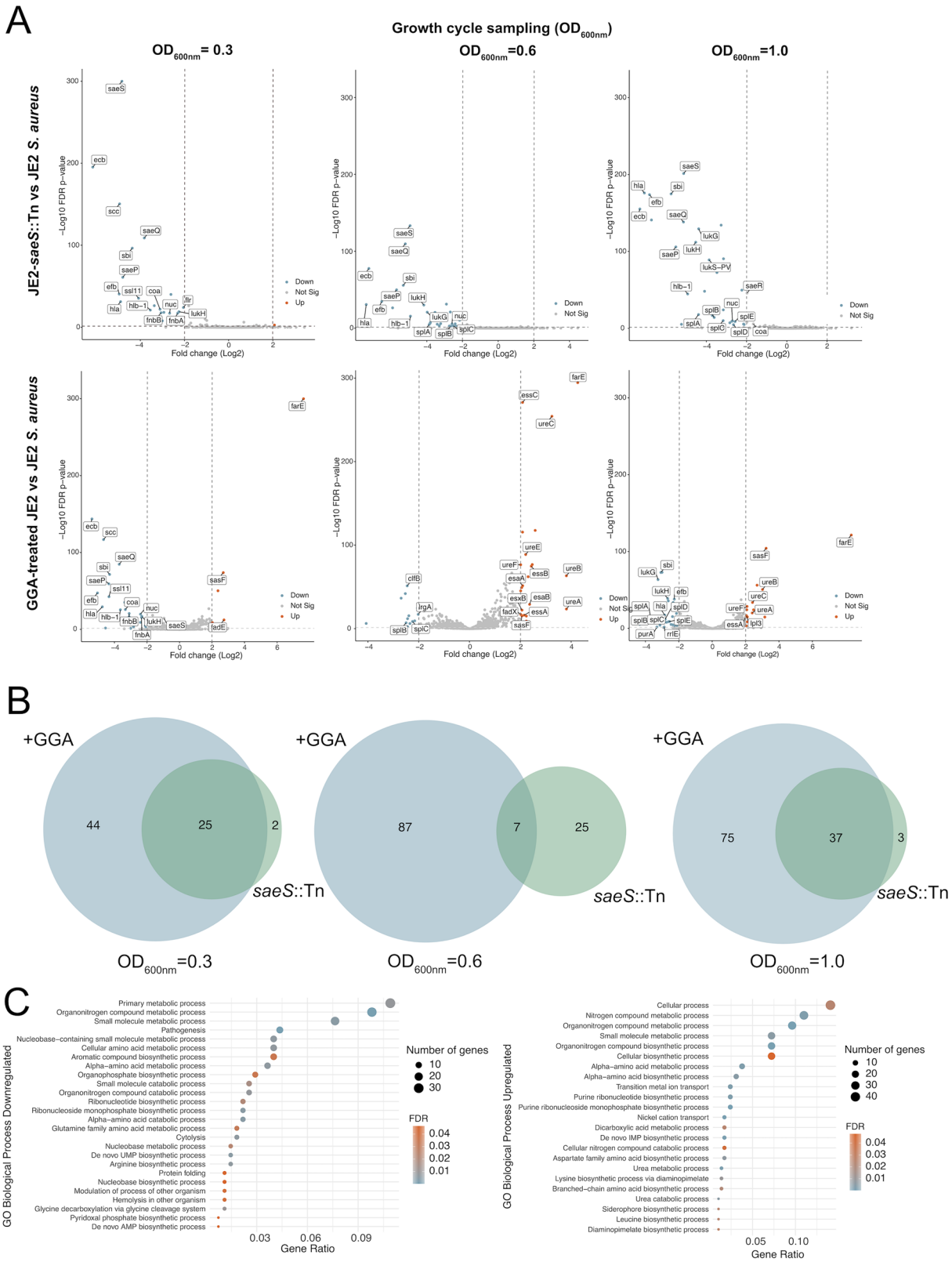

gene in response to GGA, suggesting an adaptive response to efflux the compound (Fig. 6, and Supplementary Data 3). Overall, we did not identify any further candidate regulators or pathways that could shed light on the potential targets of GGA responsible for *clfB* and *spa* reduction. Nonetheless, GGA-mediated downregulation of *clfB* and *spa*, coupled with reduced surface abundance of the CWA proteins IsdA and the FnBPs, indicates a coordinated transcriptional suppression of CWA proteins. These findings strongly suggest that GGA broadly regulates *S. aureus* virulence mechanisms by disrupting different transcriptional regulators, a focus for future studies.

GGA activity against clinical isolates and in vivo efficacy

Finally, to support future translational work, we evaluated GGA against a panel of multidrug-resistant clinical *S. aureus* isolates, representing

https://doi.org/10.1038/s41467-026-71917-8

Fig. 6 | Transcriptomic time course analysis of *S. aureus* lacking *saeS* (JE2-*saeS*::Tn), compared with GGA-treated cells, confirmed SaeRS inhibition and revealed additional transcriptional changes indicative of further cellular targets for GGA. A Volcano plots indicating MRSA USA300 JE2 (JE2) differentially expressed genes and their statistical significance in response to *saeS* disruption (JE2-*saeS*::Tn, top panels) and GGA (10 μM) treatment (bottom panels). Samples were taken at three growth stages (OD_{600nm} 0.3, 0.6, 1.0), as indicated. Significantly differentially expressed genes (two-sided, Wald test, Benjamini and Hochberg False Discovery Rate (FDR)-adjusted $P < 0.05$) are highlighted in orange (upregulated) and blue (downregulated), with the grey lines representing the boundary for identifying up- or downregulated genes. Related to Supplementary Data 3. **B** Venn diagrams depicting the overlap and unique gene sets altered by *saeS* disruption versus GGA treatment. **C** Gene ontology (GO) analysis revealed enrichment of pathogenesis-associated differentially expressed genes following GGA treatment. For this analysis, all differentially expressed genes detected across the three time points were combined. The bubble plots indicate enriched GO biological processes, with bubble size proportional to the number of genes identified in each category, and the colour scale corresponding to the false discovery rate (FDR) of each enriched process (one-sided Fisher' exact test) after Benjamini-Hochberg correction of *P*-values for multiple testing. Gene ratios were calculated by dividing the number of genes implicated in the GO biological process by the number of total input genes. The bubble plots were generated using ggplot2 in R.

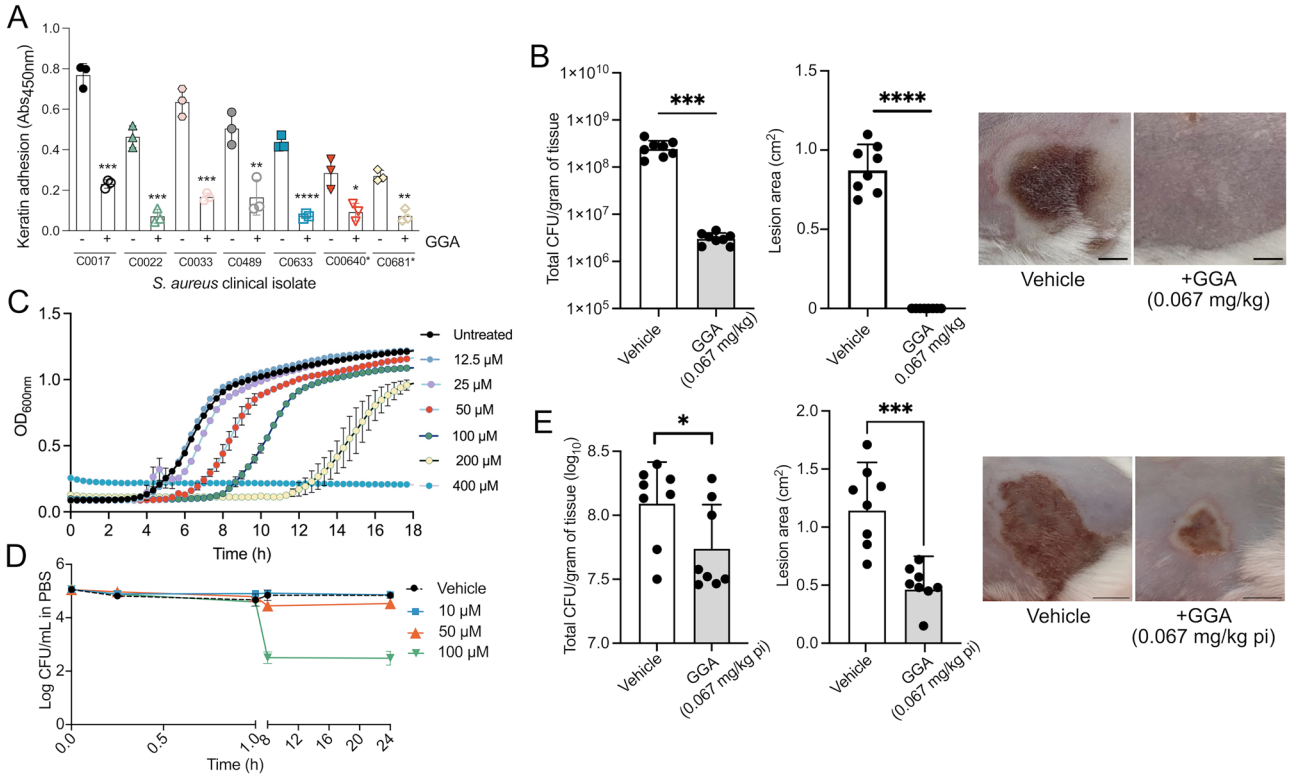

Fig. 7 | GGA anti-adhesive activity against multidrug-resistant *S. aureus* clinical isolates, antimicrobial assessment, and in vivo efficacy. A Reduction in clinical isolate adhesion (Abs_{450nm}) to keratin with GGA treatment (10 μM) ($n = 3$ biological replicates). Keratin concentrations were 0.0625 μg/well, except for isolates C0640* and C0681*, which were tested at 0.125 μg/well. Data points represent single biological replicates, and error bars represent the standard deviation (SD) of the mean. Statistical significance (two-tailed unpaired Student's *t*-test) is indicated as $P \leq 0.05$*; $P \leq 0.01$**; $P \leq 0.001$***; $P \leq 0.0001$**** compared to untreated parent strains. Related to Fig. S10 and Table S3. Exact *P* values: C017 + GGA (versus C017), $P = 0.0001$, C022 + GGA (versus C022), $P = 0.0004$, C033 + GGA (versus C033), $P = 0.0003$, C0489 + GGA (versus C0489), $P = 0.008$, C0633 + GGA (versus C0633), $P = 5.7E\text{-}05$, C0640 + GGA (versus C0640), $P = 0.019$ and C0681 + GGA (versus C0681), $P = 0.001$. **B** In a Balb/c mouse model of MRSA USA300 LAC skin and soft tissue infection (n = 8), 0.067 mg/kg GGA significantly reduced lesion size and bacterial burden (CFU) at 48 h post-infection (hpi). Mice were infected subcutaneously with 2.9×10^7 CFU mixed with vehicle or GGA, followed by a further subcutaneous 50 μL injection of GGA (0.067 mg/kg) or vehicle at 6 hpi. Each data point represents an individual lesion, and the error bars represent the SD of the measurements. Data are presented as mean values +/- SD. Statistical significance (two-tailed, unpaired *t*-test with Welch's correction) is indicated as $P \leq 0.001$*** and $P \leq 0.0001$****. Exact *P* values for total CFU/gram of tissue: GGA (versus vehicle), $P = 0.0002$ and lesion area GGA (versus vehicle), $P < 0.0001$. Representative photographs of skin lesions 48 hpi are shown. The bars equal 0.2 cm. **C** GGA susceptibility testing against the MRSA USA300 strain JE2 (JE2). Growth was measured for 18 h in the presence of increasing GGA concentrations. Data points represent the average of biological triplicates ± the SD. **D** Time-kill kinetic assays revealed that GGA exhibited time-dependent killing activity in phosphate-buffered saline (PBS). Data represent the mean ± standard deviation (SD) from three biological replicates. **E** Administration of GAA post-infection (pi) antagonized MRSA USA300 LAC in a Balb/c murine model of skin infection. Mice were infected subcutaneously with 2.9×10^7 CFU. At 1 hpi and again at 7 hpi, vehicle control and GGA (0.067 mg/kg) were administered subcutaneously at each site of infection. Each data point represents an individual lesion at 48 hpi, and the error bars represent the SD of the measurements (n = 8). Data are presented as mean values +/- SD. Statistical significance (two-tailed, unpaired *t*-test with Welch's correction) is indicated as $P \leq 0.05$* and $P \leq 0.0001$***. Exact *P* values for total CFU/gram of tissue: GGA (versus vehicle), $P = 0.030$ and lesion area GGA (versus vehicle), $P = 0.0005$. Representative photographs of skin lesions 48 hpi are shown. The bars equal 0.5 cm. Source data are provided as a Source Data file.

strains from different sources that are resistant to methicillin, fluoroquinolones, and macrolides (Table S3). Across this diverse collection, GGA consistently demonstrated anti-adhesive properties (Fig. 7A and S10).

Given the established safety profile of GGA from previous studies exploring its cancer-preventative potential[66,67], we assessed its tolerability in mice and ability to treat MRSA infections. Subcutaneous administration of 0.067 mg/kg GGA mixed with the bacterial inoculum

into depilated flanks was well-tolerated and effectively prevented the development of MRSA-induced dermonecrotic lesions (Fig. 7B). GGA administration resulted in a significant two-log reduction in bacterial burden compared to vehicle treatment, demonstrating anti-MRSA activity and a potential bactericidal effect (Fig. 7B). This prompted us to evaluate the antibacterial activity of GGA further, given that its simultaneous administration could have induced pre-inoculation bacterial killing. Susceptibility testing performed in tryptic soy broth (TSB) revealed weak antibacterial activity (minimum inhibitory concentration ≥ 200 μM) (Fig. 7C). However, while a concentration-dependent killing effect was absent when GGA was tested in TSB, killing was observed in phosphate-buffered saline (PBS), with >99.9% bacterial elimination achieved following an 8-h incubation period (Fig. 7D). These findings suggest that the in vivo efficacy of GGA may have been associated with both the disruption of virulence mechanisms and bactericidal activity against MRSA. We then demonstrated that the administration of GGA post-infection also markedly decreased the size of dermonecrotic lesions, which we posit is likely attributable to inhibition of virulence factors since the bacterial burden remains high, yet disease severity was decreased 48 h post-infection (Fig. 7E).

Discussion

Here we report the identification of GGA, a naturally occurring branched-chain polyunsaturated fatty acid (FA) produced by medicinal plants like turmeric and ginger[21], as an effective antivirulence agent. While GGA and other acyclic retinoids have been studied for their cancer-preventive properties[68–71], GGA has not previously been associated with *S. aureus* biological activity. The identified anti-adhesive activity of this compound against multiple host ligands is particularly noteworthy, as the ability of *S. aureus* to adhere to these host molecules is a key step in pathogenesis[7]. The promising in vivo efficacy observed in a mouse model of skin and soft tissue infection, coupled with its anti-adhesive activity against multidrug-resistant clinical isolates (Fig. 7), positions GGA as a promising anti-MRSA therapeutic. This potential is reinforced by GGA's demonstrated lack of toxicity in primary mammalian cell lines, its documented cancer-preventative properties, and its biosynthesis from mevalonate—a pathway present in certain mammalian cells[66], suggesting biocompatibility in therapeutic applications[67]. We also demonstrate that GGA reduces *S. aureus* adhesion to endothelial host cells, a step preceding invasion, which is linked to inflammatory cytokine release, chronic infections, protection from host defenses, and antibiotic evasion[72]. Therefore, GGA may function as an antibiotic adjuvant[73] in such scenarios, representing a promising alternative or adjunct therapy. Future studies will assess the therapeutic potential of GGA in varied infection models, examine dietary delivery routes, and determine how pH influences the compound's activity, including effects on other microbes such as coagulase-negative Staphylococcus skin commensals. pH is an important factor because body sites possess distinct pH ranges that could modulate the activity of GGA, as demonstrated by our pH-dependent assays (Fig. S2). The nasal mucosa typically has a pH of 5.5–6.5, while inflamed rhinitis rises to 7.2–8.3[74]. Blood plasma is maintained at 7.35–7.45[75], and chronic wounds frequently exhibit alkaline conditions (pH ≈ 7.5–9.0)[76]. These physiological variations imply that the efficacy of GGA will differ across compartments, potentially being most pronounced in the bloodstream and highly alkaline wound environments.

Mechanistic studies revealed that the anti-adhesive properties of GGA are linked to the modulation of *S. aureus* CWA proteins. Specifically, GGA reduced the surface abundance of several key CWA proteins, including the FnBPs, which are important for host cell invasion[77]. The reduction in FnBPs was attributed to inhibiting the SaeRS two-component system, a major regulator of >20 virulence factors in *S. aureus*[78]. GGA treatment consequently downregulated a variety of *S. aureus* virulence determinants, including hemolysins, adhesins, proteases, phospholipases, and leukocidins, through the inhibition of SaeRS (Fig. 6). Importantly, GGA treatment markedly repressed *hla*, the gene encoding α-toxin, the major determinant of dermonecrosis in SSTI[79] and a SaeRS-regulated virulence factor[80]. Consistent with this transcriptional effect, we observed a significant reduction in the size of dermonecrotic lesions in GGA-treated animals (Fig. 7). Importantly, our study suggests that GGA likely inhibits additional transcriptional regulators beyond SaeRS, as evidenced by its reduction of *clfB* and *spa*, which we show are not regulated by SaeRS. Due to the complex transcriptional regulatory networks in *S. aureus*, this possibility will be further investigated in future studies.

We demonstrated that other unsaturated FAs, at non-microbicidal concentrations, also inhibit *S. aureus* adhesion to keratin (Fig. 2) and modulate the abundance of CWA proteins, with the orientation of the double bonds in the hydrocarbon chain affecting their activity (Fig. 2). This observation aligns with previous findings showing that unsaturated FAs are more potent than saturated fatty acids at inhibiting Sae[59]. The enhanced potency of *cis*-unsaturated FAs compared to *trans*-unsaturated FAs likely stems from their structural differences: *cis*-unsaturated FAs exhibit a bent conformation due to double bond geometry, whereas *trans*-unsaturated FAs adopt a more linear structure resembling saturated FAs[81]. This conformational difference impacts the ability of FAs to modulate the molecular mechanisms regulating *S. aureus* CWA protein-encoding genes, with the kinked *cis*-unsaturated FAs proving more effective. While the precise molecular mechanism underlying GGA-mediated inhibition of transcriptional regulators requires further investigation, we hypothesize that GGA intercalates into the membrane non-covalently via hydrophobic interactions with lipid tails (Fig. 5G), despite not being incorporated into membrane phospholipids (Fig. 4). The sensor histidine kinase SaeS, an intramembrane protein lacking an extracellular domain[82] that senses environmental signals[83,84], recruits SaeP and SaeQ to regulate phosphatase activity and revert to its pre-induced state[85]. Despite extensive study of the SaeRS system, the mechanisms by which SaeS detects and processes signals remain poorly understood[78]; however, inhibition of SaeS is independent of FA membrane incorporation[59]. We propose that intercalation by unsaturated FAs with kinked hydrocarbon tails disrupts phospholipid packing, altering membrane fluidity and/or interfering with the ability of the system to sense environmental stimuli, autophosphorylate, or engage in protein-protein interactions. Consistent with this, unsaturated FAs are known to influence membrane fluidity[52,64], a factor that activates type VII secretion in *S. aureus*[64]—a system we observed upregulated by GGA. Notably, while GGA contains *trans*-configured double bonds, its extensive branching likely contributes similarly to phospholipid packing disruption. In contrast, saturated FAs and unbranched trans-FAs pack tightly without affecting our observed phenotypes. These findings underscore the complex interplay between FA structure, membrane dynamics, and signaling pathways, highlighting how specific biophysical properties of unsaturated FAs modulate membrane-associated processes.

This work further emphasizes the multifaceted role of FAs in host-pathogen interactions and reveals an unrecognized activity: FAs not only disrupt biofilm formation[24–26] but also directly inhibit *S. aureus* adhesion to host ligands, a novel finding with important therapeutic implications. Notably, many of the anti-adhesive unsaturated FAs identified here are naturally present within the human body and contribute to innate immunity[86–88]. ~15–30% of skin sebum is composed of free FAs[89] with common constituents including palmitic acid (C16:0, 31%), sapienic acid (sebum-specific C16:1, 21%), stearic acid (C18:0, 11%), myristic acid (C14:0, 10%), and oleic acid (C18:1, 8%)[86]. Free FAs are also found in the bloodstream, where concentrations—influenced by diet—can range from 100 μM to over 1 mM, with typical constituents including palmitic acid, stearic acid, oleic acid, linoleic acid, and arachidonic acid[87,88,90]. Importantly, GGA, when consumed through foods

like turmeric, is absorbed and detectable in the bloodstream[66]. This raises a compelling possibility: diet may influence *S. aureus* colonization and infection propensity, with diets rich in FAs, including those found in medicinal plants such as turmeric, potentially conferring protection. While free FAs are well known for their antibacterial properties, with growth inhibition primarily attributed to increased membrane disorder, leakage of cellular contents, and disruptions in nutrient uptake and the electron transport chain[91,92], we demonstrate that several also exhibit anti-adhesive properties at concentrations that do not impair bacterial growth or respiration[59]. This aligns with previous research showing that sapienic acid and other unsaturated FAs inhibit virulence factor production[55] while also revealing for the first time that adhesion is similarly affected. Additionally, glycerol monolaurate, a surfactant used in the food and cosmetics industry, is hydrolyzed by *S. aureus*, releasing lauric acid, which also inhibits virulence factor production[93].

In summary, our findings support fatty acids, particularly GGA, as promising anti-MRSA agents, with their antivirulence activity primarily mediated through the inhibition of transcriptional regulators. Future research should prioritize elucidating the compound's precise molecular targets, further evaluating its in vivo efficacy and synergistic potential when combined with existing antimicrobials, and carefully assessing the risk of MRSA developing resistance to this approach.

Methods

Ethics statement

All study protocols comply with the relevant ethical regulations. The animal protocols (AUP #2021-090) were performed in compliance with guidelines set out by the Canadian Council on Animal Care and reviewed and approved by the University of Western Ontario Animal Use Subcommittee.

Bacterial strains and culture conditions

All strains were propagated in microtiter plates at 37 °C with aeration (900 rpm with a 3 mm throw) or in glassware at 37 °C with aeration (220 rpm with a 25 mm throw) (INFORS HT Multitron). *S. aureus* strains were routinely cultured in tryptic soy broth (TSB; Wisent Inc.), while *Escherichia coli* strains were grown in Lysogeny broth (LB; BioShop Canada). For the experimental assays with fatty acids, *S. aureus* strains were cultured in TSB supplemented with 5 mM HEPES [pH 7.0] unless otherwise stated. MRSA USA300 JE2 NTML mutant strains harbouring the *Bursa aurealis* transposon were selected on erythromycin (5 μg/mL). To maintain the pALC2073 plasmid, the growth medium was supplemented with chloramphenicol (10 μg/mL). Information related to the clinical isolates profiled in this study can be found in Table S3, and all other bacterial strains and plasmids used in this study are provided in Table S4. Biological replicates were performed by inoculating independent single-colony cultures and assaying them on the same day (unless noted otherwise).

Construction of MRSA USA300 AH1263 KB4058

To construct the *htrA1* deletion plasmid, PCR was used to amplify fragments upstream (Primers JBHTRA1 and JBHTRA2, chromosome template) and downstream (primers JBHTRA3 and JBHTRA4, chromosome template) of *htrA1*. The upstream fragment was digested with *Eco*RI and *Bam*HI, and the downstream fragment was digested with *Bam*HI and *Sal*I. These fragments were ligated in a single step into pJB38[94] digested with *Eco*RI and *Sal*I to generate pJB170. This plasmid was then passaged through *S. aureus* RN4220 before electroporation into MRSA USA300 AH1919[95] via phi11-mediated transduction as previously described[96]. The allelic exchange was performed as previously described[94], and the Δ*htrA1* mutation was confirmed by PCR (primers JBHTRA4 and JBHTRA10). This strain was designated MRSA USA300 AH1263 KB4053. Next, an allelic exchange plasmid for *htrA2* was generated using the same cloning technique and sites. The upstream fragment used primers JBHTRA5 and JBHTRA6, while the downstream fragment used primers JBHTRA7 and JBHTRA8 to generate pJB177. This plasmid was then electroporated into MRSA USA300 AH1263 KB4053 as described above, and allelic exchange was performed. The *htrA2* mutation was confirmed using primers JBHTRA8 and JBHTRA12. Additional JBHTRA primers were used to sequence the plasmids. PCR was performed using the KOD polymerase, and DNA was purified using ZymoResearch Clean and Concentrate-5 or gel-extraction kits, according to the manufacturer's suggested guidelines. All inserts were verified by Sanger sequencing to ensure no unintended changes occurred. All primer sequences can be found in Table S5.

Anti-adhesive high-throughput compound screen

Chemical screening was performed at the McMaster University Centre for Microbial Cell Biology (CMCB). Overnight saturated cultures of MRSA USA300 JE2 and MRSA USA300 JE2-*srtA*::Tn were propagated for 18 h at 37 °C. The overnight cultures were standardized to an OD_{600nm} of 0.1 in sterile 0.85% (*w/v*) NaCl and diluted 1:200 into unbuffered TSB. 1 μL of each compound from a Bioactive Compound Library (McMaster University, Supplementary Data 1) was applied to each well of a 96-well round-bottom plate (VWR, untreated clear round bottom) for a final concentration of 10 μM (1% DMSO) using an Echo 550 acoustic liquid handler (LabCyte). Subsequently, 99 μL of the standardized inoculum was applied to each well. Compounds were profiled in technical duplicate across separate microtiter plates. Each plate also included untreated MRSA USA300 JE2 and MRSA USA300 JE2-*srtA*::Tn as adhesion-positive and negative controls, respectively. DMSO (1% *v/v*) was included as a solvent control. The bacterial strains were then propagated to an OD_{600nm} of 0.6 and irradiated under ultraviolet (UV) light for 20 min to halt growth. To measure adhesion, Nunc™ Immunosorbent (Maxisorp™) 96-well microtiter plates were coated with 100 μL of human keratin derived from the human epidermis (Millipore Sigma) at a concentration of 0.2 μg/well. The keratin was diluted in a carbonate buffer: 15 mM Na_2HCO_3, 35 mM $NaHCO_3$ [pH 9.6], and the plates were incubated at 4 °C for 18 h. Both the keratin-coated plates and the irradiated bacterial cultures were stored at 4 °C overnight. The following day, the keratin solution was removed, and the keratin-coated plates were blocked with 300 μL of 2% BSA (HyCloneTM) (*w/v*) for 1 h. Following blocking, 50 μL of the bacterial cultures and 50 μL of PBS were applied to the keratin-coated plates. The plates were sealed, agitated for 5 min (900 rpm), and incubated for 1 h with gentle shaking (100 rpm). For the final 20 min, the microtiter plate lids were removed, and the bacterial cultures were irradiated under ultraviolet (UV) light. 100 μL of a mouse IgM anti-*S. aureus* monoclonal primary antibody raised against UV-inactivated *S. aureus* (Invitrogen) (2 μg/ml in 1% BSA) was applied to each well, and the plates were agitated for 5 min (600 rpm), followed by 1 h incubation with gentle shaking (100 rpm). 100 μL of a secondary anti-mouse IgM goat HRP-conjugated antibody (Invitrogen) (125 ng/ml in 1% BSA) was then applied as described for the primary antibody. Between each described step, the plates were incubated at room temperature and washed four times with 300 μL of PBS [pH 7.4], except for host ligand aspiration, where the plates were only washed once with 300 μL of PBS. Adhesion was assessed using 100 μL of room temperature equilibrated 3,3',5,5'-tetramethylbenzidine (TMB) colorimetric substrate (BioLegend), which was agitated for 1 min (600 rpm), followed by gentle shaking (100 rpm) for 20 min. The reaction was quenched by oxidation with 100 μL of 2 M H_2SO_4. Absorbance was measured at 450 nm using a BioTek Synergy H1 microplate reader. Growth (OD_{600nm}) and adhesion (Abs_{450nm}) were normalized using the interquartile mean (IQM) method and the mean of the inner two quartiles of ranked data, reducing influence from outliers and plate-to-plate variation[20].

ELISA-based adhesion assay

The ELISA-based adhesion assays were performed as previously described[12]. Briefly, Maxisorp microtiter plates (Thermo Scientific)

were coated with 100 μL of host ligand and incubated at 4 °C for 18 h. Keratin (Millipore Sigma) was diluted in carbonate buffer (15 mM NaHCO, 35 mM NaHCO [pH 9.6]). Fibronectin and fibrinogen (Millipore Sigma) were diluted in phosphate-buffered saline (PBS) [pH 7.4]. The following day, the liquid was aspirated from the plate, the wells were washed with PBS and then blocked with 300 μL of 2% BSA (HyCloneTM) (*w/v*) for 1 h. Following blocking, 100 μL of the bacterial cultures was applied to the coated plates. For the adhesion assays, bacterial strains were routinely grown to an OD_{600nm} of ~0.4 for fibronectin, ~0.6 for keratin, and ~1.0 for fibrinogen. When optimizing pH, TSB was supplemented with 5 mM HEPES [pH 7.0], 5 mM HEPES [pH 8.0], 50 mM bis-tris propane [pH 9.0], or 100 mM MES [pH 5.5]. The plates were sealed, agitated for 5 min (900 rpm), and incubated for 1 h with gentle shaking (100 rpm). For the final 20 min, the microtiter plate lids were removed, and the bacterial cultures were irradiated under ultraviolet (UV) light. The plates were then washed, and 100 μL of PBS was added before irradiating the plate under UV light for an additional 20 min. The PBS was removed, and 100 μL of a mouse IgM anti-*S. aureus* monoclonal primary antibody raised against UV-inactivated *S. aureus* (Invitrogen) (2 μg/ml in 1% BSA) was applied to each well. The plates were agitated for 5 min (600 rpm), followed by 1 h incubation with gentle shaking (100 rpm). 100 μL of a secondary anti-mouse IgM goat HRP-conjugated antibody (Invitrogen) (125 ng/ml in 1% BSA) was then applied as described for the primary antibody. Between each described step, the plates were incubated at room temperature and washed four times with 300 μL of PBS [pH 7.4], except for host ligand aspiration, where the plates were only washed once with 300 μL of PBS. Adhesion was assessed using 100 μL of room temperature equilibrated TMB colorimetric substrate (BioLegend), which was agitated for 1 min (600 rpm), followed by gentle shaking (100 rpm) for 20 min. The reaction was quenched by oxidation with 100 μL of 2 M H_2SO_4. Absorbance was measured at 450 nm using a BioTek Synergy H1 microplate reader.

Assessing lead compound potency

GGA was resupplied (Cayman Chemicals) to further assess anti-adhesive potential. Cultures were grown overnight for 18 h and diluted 1:100 into unbuffered TSB. GGA was titrated 1.5-fold in 96% ethanol (*v/v*) starting at a high dose of 50 μM and the culture was propagated to an OD_{600nm} of 0.6. For comparison, MRSA USA300 JE2 and MRSA USA300 JE2-*srtA*::Tn were included on each plate as positive and negative adhesion controls, respectively. The ELISA to investigate keratin adhesion was performed as described.

Assessing the anti-adhesive activity of GGA against *S. aureus* clinical isolates

Keratin adhesion assays of *S. aureus* clinical isolates were performed using the ELISA-based adhesion assay described above. We selected clinical *S. aureus* isolates with resistance to ≥ six antibiotics from the Wright Clinical Collection at McMaster University. These isolates were obtained from different patients on separate days and represented diverse infection sites. Each isolate was incubated in TSB overnight at 37 °C. The overnight culture was diluted 1:100 into 5 mL TSB ± GGA (10 μM) and grown to an OD_{600nm} of ~0.6. Once the appropriate OD_{600nm} was reached, 100 μL of each isolate was applied to keratin-coated Nunc™ Immunosorbent (Maxisorp™) 96-well microtiter plates, and the ELISA was performed as described above. The Abs_{595nm} was measured using a BioTek Synergy H1 microplate reader.

Fatty acid susceptibility profiling

Single colonies were used to inoculate TSB in biological triplicate and propagated overnight at 37 °C. The cell inoculum was prepared by standardizing all strains to an OD_{600nm} of 0.1 in 0.85% (*w/v*) NaCl, followed by a 1:200 dilution into TSB. To assess the susceptibility of MRSA USA300 JE2 to exogenous FAs, each FA was titrated 2-fold, starting at 200–500 μM (1% solvent). Myristelaidic acid (Millipore Sigma), palmitic acid (Sigma Aldrich), oleic acid (EMD Millipore), elaidic acid (Cedarlane Labs), linoleic acid (Sigma Aldrich), linoelaidic acid (Cedarlane Labs), linolenic acid (Cedarlane Labs), and arachidonic acid (Cedarlane Labs) were dissolved in 100% DMSO. Myristic acid (Cedarlane Labs), palmitoleic acid (Fisher Scientific), stearic acid (Sigma Aldrich), and GGA were dissolved in 96% (*v/v*) ethanol. Arachidic acid (Millipore Sigma) was dissolved in 100% acetone. The plates were incubated at 37 °C with linear shaking (3 mm throw), and the OD_{600nm} was measured every 15 min for 18 h using a BioTek Synergy H1 microplate reader. The MIC values were determined by identifying the lowest concentration of the compound where the OD_{600nm} value was <0.1 after correcting for the initial OD_{600nm}.

Fatty acid dose-dependent adhesion assays

Fatty acid adhesion assays were performed as described above with minor adjustments. Three biological replicates of MRSA USA300 JE2 and MRSA USA300 JE2-*srtA*::Tn were grown overnight for 18 h. Strains were subcultured 1:100 into 5 mL TSB supplemented with each fatty acid (FA) (10 μM) and grown to the desired OD_{600nm} (0.4 for fibronectin, 0.6 for keratin, and 1.0 for fibrinogen). MRSA USA300 JE2-*srtA*::Tn was included as an adhesion-defective, untreated negative control. Once the appropriate OD_{600nm} was reached, 100 μL of each strain was applied to each well, and the ELISA was performed as described above. FAs that did not attenuate adhesion at 10 μM were profiled at the highest concentration possible based on their solubility limit and MIC: myristic acid (100 μM), myristelaidic acid (50 μM), palmitic acid (100 μM), stearic acid (100 μM), and arachidic acid (75 μM). For crystal violet detection of adhesion, following UV irradiation, 100 μL 0.5% (*w/v*) crystal violet [20% (*v/v*) methanol] was applied to each well and incubated at room temperature for 4 min. The crystal violet was removed, washed four times with 400 μL PBS, and solubilized using 7% (*v/v*) acetic acid. The Abs_{595nm} was measured using a BioTek Synergy H1 microplate reader.

Measuring the abundance of CWA proteins on the surface of *S. aureus*

CWA protein surface abundance was measured using a previously described ELISA-based adhesion assay[12]. These assays were performed in bacterial strain backgrounds devoid of the *S. aureus* immunoglobulin binding proteins, SpA and Sbi (MRSA USA300 JE2-*sbi*::Tn and MRSA USA300 JE2-Δ*spa*Δ*sbi*) unless otherwise stated. Three biological replicates of each strain were grown overnight at 37 °C for 18 h. Overnight cultures were diluted 1:100 into 5 mL of TSB. FAs were added to a final concentration of 10 μM. For FnBP and SpA detection, the bacterial strains were grown to an OD600nm of ~0.4 and 1.0, respectively[12,13]. For IsdA detection, three biological replicates of MRSA USA300 JE2, MRSA USA300 JE2 + 10 μM GGA, and MRSA USA300 JE2-*isdA*::Tn Δ*spa*Δ*sbi* were propagated overnight in TSB supplemented with 0.5 M 2,2′-dipyridyl (DIP) (Fisher Scientific) to limit iron availability and promote *isdA* expression. Once the desired OD_{600nm} was achieved, all strains were harvested by centrifugation at 4,000 *x g* for 10 min at 4 °C, washed once in PBS, and standardized in PBS to an OD_{600nm} of 2.0.

The standardized bacterial cultures were applied to Nunc Maxisorp™ microtiter plates and diluted 2-fold in PBS. The plates were sealed and agitated for 5 min (900 rpm), followed by incubation for 1 h at room temperature with gentle shaking (100 rpm). During the final 20 min of incubation, the microtiter plate lids were removed, and the cultures were irradiated under ultraviolet (UV) light for 20 min. Then, 100 μL of PBS was applied before irradiating under UV light for a further 20 min. The PBS was aspirated, and 300 μL 2% (*w/v*) BSA (in PBS) was applied to each well, followed by static incubation for 1 h at room temperature. To ensure the different strains equally adhered to the plates, two identical Maxisorp plates were prepared for all the strains:

one plate was used to detect CWA protein surface abundance (described below), and the other plate was used to assess the adherence of the bacteria to the plate using crystal violet, as described above.

ELISA-based detection of CWA surface proteins was performed as previously described with the following modifications: to detect SpA, an IgG rabbit anti-mouse (H + L) HRP-conjugated secondary antibody (Invitrogen) (1:700,000 in 1% BSA) was applied to the immobilized cells. To measure the abundance of surface-exposed FnBPs, a mouse anti-FnBPAB primary antibody[12] (1:50,000 dilution in 1% (*w/v*) BSA) and 100 μL F(ab′)2 fragment goat anti-mouse IgG (H + L) HRP-conjugated secondary antibody (Jackson ImmunoResearch) (1:20,000 in 1% (*w/v*) BSA) were applied to each well. IsdA was detected using an anti-IsdA polyclonal rabbit antibody[34] and a goat anti-rabbit HRP conjugated secondary antibody (Invitrogen), both diluted 1:100,000 in 1% (*w/v*) BSA.

Immunoblotting sample preparation

Strains of interest were assessed in biological triplicate and grown overnight in 3 mL of TSB for 18 h at 37 °C. An MRSA USA300 JE2-Δ*spa*Δ*sbi* background was utilized for the detection of FnBPs, and an MRSA USA300 JE2-Δ*sbi* background was used for the detection of SpA. Overnight cultures were diluted 1:100 into 10–20 mL of TSB and propagated to the appropriate OD_{600nm}. The cells were harvested by centrifugation at 4000 × *g* for 10 min at 4 °C and washed once with PBS. The cell pellet was suspended in 400 μL tris-buffered saline with EDTA-free Pierce™ protease inhibitor minitablets (TBSI, 50 mM Tris-HCl [pH 7.5], 100 mM NaCl), and the cells were lysed with 30 μg/mL of lysostaphin for 45 min at 37 °C until the sample was translucent. Following lysis, the samples were stored at −20 °C. Culture supernatants were collected following centrifugation and passed through a 0.2 μm pore filter to remove any bacterial cells. The supernatants were concentrated using Amicon Ultra-15 10,000 Da MWCO (SpA) and 30,000 Da MWCO (FnBPs) centrifugal filter units (Millipore Corporation) to ~100–400 μL and stored at −80 °C.

Western immunoblotting

Immunoblotting was performed as previously described[12], with minor changes. The whole cell samples were quantified using a BCA assay (Pierce), and the supernatant samples were quantified using a Bradford protein assay (Biorad). 1–5 μg of protein from each sample (1 μg for supernatant samples and 5 μg for whole cell samples) was boiled with 4× Laemmli loading buffer, and the proteins were resolved using SDS–PAGE and 4 to 15% Mini-PROTEAN TGX Precast Stain-Free acrylamide gels (BioRad). Before transfer, the gels were activated for 5 min using the Stain-Free gel protocol. The proteins were transferred overnight onto LF-PVDF membranes (BioRad) at 4 °C (20 V) using a wet transfer apparatus. Following the transfer, the membranes were blocked for 1 h with 5% (*w/v*) skim milk in TBS (10 mM Tris-HCl [pH 7.5], 150 mM NaCl). To detect SpA, the membrane was incubated for 1 h with a rabbit anti-mouse IgG (H + L) HRP-conjugated secondary antibody in 5% (*w/v*) skim milk in TBST (10 mM Tris-HCl [pH 7.5], 150 mM NaCl, 0.01% Tween 20) (1:20,000), followed by three washes with TBST. To quantify the abundance of FnBPs, the mouse anti-FnBPAB antibody [1:2000 in 5% (*w/v*) skim milk in TBST] was incubated with the membrane for 1 h, washed three times with TBST, and then incubated for 1 h with a peroxidase AffiniPure F(ab′)2 fragment goat anti-mouse IgG (H + L) HRP-conjugated secondary antibody (1:3,000 in TBST, 5% (*w/v*) skim milk; Jackson ImmunoResearch). To quantify the abundance of SpA, the membrane was incubated for 1 h with a rabbit anti-mouse IgG (H + L) HRP-conjugated antibody (Invitrogen) in 5% (*w/v*) skim milk in TBST. To measure total protein, the membrane was imaged using the Stain-Free blot protocol (Biorad) and then developed using Immobilon Crescendo western chemiluminescent HRP substrate (Millipore Sigma). The blots were visualized using a Biorad ChemiDoc XRS+ system. Protein intensity was normalized to the total protein using ImageLab and Stain-Free technology (BioRad).

Atomic force microscopy (AFM)

A single colony was inoculated into 10 mL TSB and incubated overnight at 37 °C with aeration (180 rpm). Bacteria were collected by centrifugation (2000 ×*g*, 5 min), washed with TSB, diluted in the same medium supplemented with 5 mM HEPES (pH 7) to an OD_{600nm} of 0.05, and propagated to the exponential phase of growth (OD_{600nm} of 0.6) in the absence or presence of 10 μM of GGA or linoleic acid. Afterward, the cells were harvested by centrifugation and washed twice with PBS. The cell suspension was diluted 100 times and deposited on a polystyrene dish for 20 min, then gently rinsed with PBS before AFM measurements.

AFM probe functionalization

Gold-coated cantilevers (PNP-Tr-Au, Nanoworld) were functionalized with human fibronectin (Sigma-Aldrich). Before functionalization, cantilevers were thoroughly rinsed with water and ethanol, dried with N_2 flow, and further cleaned in a UV-ozone chamber for 10 min. They were then immersed overnight in a 1 mM solution containing a mixture of 16-mercaptododecahexanoic acid (10%; Sigma-Aldrich) and 1-mercapto-1-undecanol (90%; Sigma-Aldrich) in ethanol and protected from light. Then, the cantilevers were rinsed with ethanol, dried with N_2, and immersed in an aqueous solution containing 10 mg/mL *N*-hydroxysuccinimide (NHS) and 25 mg/mL 1-ethyl-3-(3-dimethylaminopropyl)-carbodiimide (EDC) for 30 min. After rinsing with ultrapure water, the cantilevers were immersed in a 0.1 mg/mL fibronectin solution in PBS for 1 h and finally rinsed with PBS.

Single-molecule force spectroscopy (SMFS)

The affinity of individual *S. aureus* cells for human fibronectin was evaluated through AFM-based SMFS using fibronectin-functionalized AFM probes. Experiments were performed in PBS, at room temperature, using JPK NanoWizard®V NanoScience AFM. Fibronectin-functionalized cantilevers were calibrated using the thermal noise method[97], yielding spring constants in the 0.02–0.04 N/m range. Force-distance curves were recorded on the top of single bacterial cells (500 × 500 nm^2 areas) in force mapping mode (32 ×32 force curves) using a constant approach and retraction speeds of 1 μm/s, 1 μm ramp length, applying a force of 250 pN. All force curves were analyzed using JPK Data Processing software (version 8.0.144), considering the last adhesion peak, which was fit using the worm-like chain model of polymer extension[98]. Adhesion force and rupture length values were plotted as histograms for each cell, and the average values were extracted by fitting with a Gaussian function. Adhesion probability was calculated by the ratio between the number of force curves showing a specific adhesion event and the total number of curves collected per cell. Statistical analysis was carried out using Origin software (OriginPro 2021).

Assessing *S. aureus* protease production

Secreted protease production in the presence of unsaturated FAs was analyzed using SDS-PAGE as previously described[41]. MRSA USA300 AH1623 treated with linoleic acid (10 μM) was used as a positive control since this fatty acid is known to induce the Staphylococcal Proteolytic Cascade[41], and the protease-deficient strain MRSA USA300 AH1623 KB4058 (KB4058) was included as a negative control. Single colonies of MRSA USA300 strain AH1263 were inoculated into 3 mL of TSB in the presence and absence of FAs (10 μM linoleic acid or 10 μM GGA), followed by incubation for 18 h at 37 °C in biological triplicate. The overnight cultures were harvested by centrifugation, and the supernatants were collected. Secreted proteins in the cell-free supernatants were precipitated with trichloracetic acid (TCA) (10% (*v/v*)) for 30 min on ice. Samples were harvested by centrifugation at 18,000 × *g* (4 °C)

and washed in 70% ethanol before air drying. Once dry, the samples were dissolved in 200 μL of 1x Laemmli loading buffer. Proteins derived from 2.0 OD_{600nm} units of precipitated supernatant were resolved on a 12% acrylamide gel and visualized by Coomassie staining. The gel was imaged using a Biorad ChemiDoc XRS+ system. A BSA standard curve was used to correlate band density to protein concentration. Band density was quantified using ImageLab. Protein abundance of pro-Geh was calculated based on the linear equation generated from the standard curve.

To assess whether secreted proteases impact GGA-mediated inhibition of keratin adhesion, overnight cultures of MRSA USA300 AH1623 and MRSA USA300 AH1623 KB4058, a mutant strain devoid of all proteases, were treated with and without 10 μM GGA and propagated to an OD_{600nm} of 0.6. All cultures were applied to keratin-coated Maxisorp plates, and dose-dependent adhesion was measured using the ELISA-based adhesion assay described above.

Scanning electron microscopy

Strains of interest were propagated in TSB to an OD_{600nm} of 0.6. The cells were harvested by centrifugation (4000 × *g*, 4 °C) and washed three times in 0.85% (*w/v*) NaCl. The samples were adhered to carbon planchets, fixed with 2.5% (*v/v*) glutaraldehyde (1 h) and 1% osmium tetroxide (30 min), dried under ambient conditions, and coated with 15 nm of gold using a sputter coater (Denton Desk V TSC). Images were acquired using an FEI Quanta FEG 250 scanning electron microscope (ThermoFisher Scientific) operated at 5.0 kV under high vacuum.

Lipidomics analysis

Overnight cultures of five biological replicates of MRSA USA300 JE2 were diluted 1:100 into 20 mL of TSB ± 10 μM GGA and grown to an OD_{600nm} of 1.0. The cells were harvested by centrifugation, and the cell pellet was washed in 1.5 mL Buffer A (100 mM potassium phosphate [pH 7.2], 5 mM EDTA). The pellet was washed with 1.5 mL Buffer B (100 mM potassium phosphate [pH 8.2], 600 mM KCl) three times and harvested by centrifugation at 21,000 × *g* for 5 min. For the final wash, the cells were harvested by centrifugation at 4 °C at 4000 × *g* for 5 min. The pellet was resuspended in 1.8 mL ice-cold Buffer C (200 mM potassium acetate [pH 4.5], 600 mM KCl), transferred into a pre-weighed glass vial, and harvested by centrifugation at 1000 × *g* for 10 min. Following each wash, the pellet was resuspended in chloroform: methanol (20 uL per 1 mg of the pellet) and mixed gently for 2 h at room temperature. The pellet was harvested by centrifugation at 1000 × *g* for 10 min. Following centrifugation, the supernatant was transferred to a clean, preweighed glass vial, and 0.9% NaCl was applied to a final concentration of 20% (*v/v*) to induce phase separation. The mixture was gently mixed for 10–15 min and then harvested by centrifugation for 10 min at 1000 × *g*. The methanol layer (top) was discarded, and the chloroform layer (bottom) containing the lipids was stored at −20 °C.

The Kansas Lipidomics Research Center Analytical Laboratory analyzed phosphatidylglycerol (PG). Phospholipid and galactolipid internal standards were included: 0.6 nmol phosphatidylcholine (PC) (di12:0), 0.6 nmol PC (di24:1), 0.6 nmol lysophosphatidylcholine (LPC) (13:0), 0.6 nmol LPC(19:0), 0.3 nmol phosphatidylethanolamine (PE) (di12:0), 0.3 nmol PE (di23:0), 0.3 nmol lysophosphatidylethanolamine (LPE) (14:0), 0.3 nmol LPE(18:0), 0.3 nmol PG (di14:0), 0.3 nmol PG (di20:0(phytanoyl), 0.3 nmol lysophosphatidylglycerol (LPG) (14:0), 0.3 nmol LPG (18:0), 0.287 nmol phosphatidylinositol (PI) (16:0–18:0), 0.105 nmol PI (di18:0), 0.2 nmol phosphatidylserine (PS) (di14:0), 0.2 nmol PS (di20:0(phytanoyl)), 0.3 nmol phosphatidic acid (PA) (di14:0), 0.3 nmol PA (di20:0(phytanoyl)), 3.1 nmol triacylglycerol TAG (tri17:1), 0.44 nmol digalactosyldiacylglycerol (DGDG) (16:0–18:0), 1.48 nmol DGDG (di18:0), 1.665 nmol monogalactosyldiacylglycerol (MGDG) (16:0–18:0), diacylglycerol (DAG) (15:0) 4.64 nmol, and 1.405 nmol MGDG (di18:0).

The sample and internal standard mixture were combined with solvents such that the ratio of chloroform, methanol, and 300 mM ammonium acetate in water was 360/100/5:25, with a final volume of 1.4 mL. Analysis of PG in positive and negative ion mode was performed on unfractionated lipid extracts introduced by direct infusion into the electrospray ionization (ESI) source on a linear ion trap quadrupole LC-MS/MS (QTrap 6500+ Low Mass; AB Sciex Instruments, Concord, ON). The data were corrected for the fraction of the sample analyzed and normalized to the signal per OD_{600nm}, such that 1.0 OD_{600nm} unit equalled 1.0 nmol of internal standard. For normalization, each peak's signal was compared to that of the internally spiked phospholipid standards, added at the quantities indicated above. The data was quantified using the LipidomeDB Data Calculation Environment (http://lipidome.bcf.ku.edu:8080/Lipidomics/).

SaeRS activity assay

β-Galactosidase activity was measured as described previously, with minor modifications[57,59,99]. Overnight cultures of MRSA USA300 AH1263 with the P_{coa}-*lacZ* reporter plasmid pJB1018[57] were diluted to an OD_{600nm} of 0.1 in 5 mL of TSB ± 10 μM GGA and 31.4 μM oleic acid diluted in 95% (*v/v*) ethanol. 95% (*v/v*) ethanol was used as a solvent control. After 5.5 h, cells from 1 mL of culture were harvested and stored at −80 °C until the assay was performed. The cell pellet was suspended in 1.2 mL Z-buffer (60 mM Na_2HPO_4, 40 mM NaH_2PO_4, 10 mM KCl, 1 mM $MgSO_4$, 50 mM β-mercaptoethanol, [pH 7.0]) and disrupted using a FastPrep-24 5 G homogenizer (MP Biomedicals) with 0.1 mm glass beads at 6.0 m/s for 2 cycles of 40 s. Each sample was incubated on ice for 300 s between cycles. Cellular debris was harvested by centrifugation at 21,130 × *g* for 5 min, and the lysate was transferred to a new tube. (50–200 μL of the lysate was removed and combined with Z-buffer for a total volume of 700 μL to which 140 μL *o*-nitrophenyl β-D-galactopyranoside (ONPG) (4 mg/mL (*w/v*, in 40 mM NaH_2PO_4, 60 mM Na_2HPO_4, [pH 7.0])) was applied and incubated statically at 37 °C until the sample turned slightly yellow. At this point, 200 μL of 1 M $NaCO_3$ was used to quench the reaction, and absorbance was measured at 420 nm. A sample of cell lysate was used for protein quantification using the Protein Assay Dye Reagent (Bio-Rad, Hercules, CA) following the manufacturer's guidelines. Modified Miller Units were determined using protein content instead of the optical density of cells.

Endothelial cell adhesion assay

Endothelial cell adhesion assays were performed as previously described, with minor modifications[100]. HMEC-1 endothelial cells (ATCC CRL3243) were cultured at 37°C in 5% CO_2 in MCDB 131 medium (Gibco) supplemented with human Epidermal Growth Factor (10 ng/mL), hydrocortisone (1 μg/mL), glutamine (10 mM) and 10% (v/v) fetal bovine serum (FBS). One day prior to infection, the HMEC-1 cells were split using trypsin to generate and single suspension of HMEC-1 cells, which were seeded into 12 well tissue culture dishes and grown for 24 h in the medium described above. At this time, the wild-type *S. aureus* strain USA300 and a Δ*fnbAB* mutant were inoculated into TSB and grown overnight with aeration at 250 rpm at 37 °C. The next day, the cultures were diluted 1:100 into 3 mL of TSB (5 mM HEPES, pH 7.0), supplemented with either GGA (10 μM) or vehicle control (95% ethanol), in sterile 13 mL polypropylene snap cap tubes. The Δ*fnbAB* bacteria were only grown in TSB. The bacteria were then propagated for 1 h and 45 min with aeration at 250 rpm at 37 °C until an OD_{600nm} of 0.4 was achieved. Next, the bacterial cells were harvested by centrifugation, washed once with 1 mL of sterile saline (0.9%, w/v NaCl), and resuspended in 1 mL of serum-free MDCB 131 tissue culture medium without supplements. The bacteria were then diluted accordingly into the same serum-free MDCB 131 medium to generate bacterial cell suspensions containing ~2.5 ×106 CFU/mL. Next, 1 mL of the bacterial suspension was applied to 12-well tissue culture plates containing ~4.5

$\times 10^5$ HMEC-1 cells per well corresponding to a multiplicity of infection (MOI) of ~5. The tissue culture plates infected with bacteria were incubated for 10 min on an orbital shaker set at 50 rpm at 37 °C. After 10 min, the plates were washed twice with 1 mL of sterile PBS at room temperature. Next, the PBS was aspirated, and the HMEC-1 cells/bacteria were incubated for ~5 min in 0.5 mL of 0.1% (v/v) Triton X-100 to create cell lysates to determine the number of adhered bacteria. The lysate was then serially diluted and drop-plated onto TSA to determine the CFU/mL for each suspension. The bacterial input for each biological replicate was also determined by serially diluting and drop-plating the starting bacterial suspensions onto TSA. The plates were incubated overnight at 37 °C, and the colony-forming units were manually enumerated.

Fatty acid kinase (Fak) complex activity assay

FakA was purified using a GST-tag, which was removed before the assay; FakB2 protein was purified using a His-tag, and the FAK assay was performed as described previously[54] with minor modifications. The Universal Kinase Kit (R&D Systems, Cat #: EA004) was used following the adjusted manufacturer's instructions. The substrate mix was prepared in the wells of a 96-well plate in triplicate by combining 10 µL of ATP (1 mM) (or ADP for the positive control) with 15 µL of oleic acid or GGA (5 mM in MeOH) in each well. The enzyme mix was prepared by combining 10 µL of coupling phosphatase (5 ng·µL^{-1}) with 7.5 µL FakA (8 µM) and 7.5 µL FakB2 (8 µM). The enzyme and substrate mixes were combined in each well, and the reaction was incubated at room temperature for 30 min with a control well consisting of only the assay buffer. 30 µL Malachite Green Reagent A, 100 µL deionized water, and 30 µL Malachite Green Reagent B were subsequently added, mixed, and then incubated at room temperature for 20 min. Abs_{620nm} was measured using a Tecan Spark 10 M plate reader to determine phosphate production and inorganic phosphate levels. The kinase activity of the Fak complex converts ATP to ADP, which is subsequently converted to AMP and inorganic phosphate by the coupling phosphatase. It is the inorganic phosphate that interacts with malachite green for the colorimetric change measured at 620 nm. In all assays, an ADP control was included.

Reverse transcription-quantitative PCR (RT-qPCR)

RT-qPCR experiments were conducted in accordance with the MIQE Guidelines[101]. Overnight cultures of MRSA USA300 AH1263 and mutant strains were diluted 1:100 in TSB or TSB supplemented with 10 µM of GGA, including at least three biological replicates. The strains were propagated at 37 °C with aeration at 220 rpm until an OD_{600nm} of 1 was achieved for *spa* and an OD_{600nm} of 0.6 for *clfB*. RNA extractions were performed using the Luna PuroSPIN Total RNA purification kit (Luna Nanotech) with some modifications in the cell lysis step. Specifically, the bacterial cells from 1 mL of the cultures were harvested by centrifugation at 12,000 × *g* for 2 min and resuspended with 100 µL of 1% lysozyme in Tris-EDTA buffer and 100 µg/mL lysostaphin, followed by incubation at 37 °C for 30 min. Following cell lysis, 250 µL of LB-R buffer (as provided in the kit) and 350 µL of molecular biology-grade ethanol were added to the lysed cells, which were then transferred to the spin columns (Luna Nanotech). The concentration and quality of RNA eluted in nuclease-free H_2O were determined using a BioTek Take3 microvolume plate (Agilent) and an Agilent BioTek Synergy H1 plate reader. To synthesize cDNA, RNA samples were standardized to ~1000 ng before removing genomic DNA using the gDNA removal reagent provided in the HiScript III RT supermix for qPCR kit (GeneBio Systems). A negative reverse-transcriptase control reaction was prepared to check for genomic DNA contamination in subsequent qPCR experiments.

Primers (Table S5) designed to amplify ~100 bp products within the genes of interest, *spa* and *clfB*, and the reference gene, *rpoD*, were assessed for specificity of binding by conducting a melt curve analysis. Single peaks were observed for all three primer pairs. Reactions were performed in MicroAmp EnduraPlate Optical 96-well Clear Reaction plates (Applied Biosystems) using the QuantStudio 3 Real-Time PCR System (Applied Biosystems) set to detect SYBR green dye (GB-Amp SYBR Green qPCR Master Mix, GeneBio Systems) and Rox (low) as the passive reference dye. A five-point standard curve with the following characteristics was used to determine the optimal amount of input cDNA: a primer efficiency of 90–100%, a slope within −3.58 and −3.10 and $R^2 > 0.99$. The negative reverse-transcriptase and no-template controls did not have significant amplification. There was also insignificant amplification detected from cDNA generated from a clean deletion mutant in the gene of interest (either Δ*spa* or Δ*clfB*). An interplate calibrator consisting of wildtype (AH1263) cDNA, aliquoted across multiple tubes to reduce freeze thaw, was included to compare data generated on different days or plates. Relative quantification of transcript expression was performed using the $2^{-\Delta\Delta Ct}$ method. The qPCR reactions were conducted in biological and technical triplicate. The average relative fold change in gene expression was determined in comparison to the untreated wildtype strain (AH1263).

Total RNA isolation and RNA-sequencing

For the transcriptomics conducted with samples harvested at an OD_{600nm} of 0.6 (in the presence and absence of 10 µM GGA), overnight saturated cultures of MRSA USA300 JE2 were diluted 1:100 into 5 mL of TSB and grown to an OD_{600nm} of 0.6 ± 10 µM of GGA. Total RNA was extracted using the RNeasy Mini Kit (Qiagen) according to the manufacturer's suggested guidelines with some modifications. 0.45 OD_{600nm} units of cells were harvested by centrifugation for 2 min at 5500 rpm. The cell pellet was incubated with 100 µL of Solution A (99 µL of TE buffer supplied in the kit, 1 µL of lysozyme (50 mg/mL in DEPC-treated H_2O)) supplemented with 20 µL of lysostaphin (5 mg/mL) for 1 h at 37 °C to lyse the cells. Following lysis, 350 µL of Solution B (350 µL of RLT, 3.5 µL of β-mercaptoethanol) and 250 µL of 100% ethanol were added. Following washing, to remove any residual buffer or ethanol, the column was dried by centrifugation (15 s at 8000 × *g*). The RNA samples were eluted in DEPC-treated H_2O and treated with TURBO DNase. The purity and quality of the RNA samples were assessed using an Agilent TapeStation 4150. All samples had a RIN^e score of 6.4–7.7. The cDNA library preparation, rRNA depletion, and Illumina RNA sequencing (12 M paired end reads) were performed by SeqCenter (Pittsburgh, PA).

For the additional time points and when evaluating the *saeS*::Tn mutant, overnight cultures of MRSA USA300 JE2 and JE2-*saeS*::Tn were propagated from single colonies inoculated into TSB or TSB+ erythromycin (5 µg/mL), respectively. The cultures were diluted 1:100 into 5 mL of TSB and sub-cultured to an OD_{600nm} of 0.3, 0.6 and 1.0 +/- 10 µM GGA. Total RNA was extracted using the Luna PuroSPIN Total RNA purification kit (Luna Nanotech) as described in the RT-qPCR method. Genomic DNA was removed using the on-column DNase treatment step. The quality of the RNA samples was evaluated by RIN^e scoring (7.2–9.4) using the Agilent TapeStation 4150 system. The samples were enriched through rRNA depletion. Subsequently, cDNA library preparation, paired-end sequencing (Illumina NextSeq 1000), demultiplexing, adapter trimming and quality control of raw reads steps were performed by the Advanced Analysis Centre at the University of Guelph, Ontario, Canada.

Differential gene expression analysis

Bioinformatics analysis was performed using software packages accessed through the public server usegalaxy.org (version 24.2.rc1). The data analysis pipeline has previously been described[102]. Quality control of raw reads, demultiplexing, and adapter trimming were completed in advance by the SeqCenter. Reads were aligned to the USA300 reference genome (GenBank: CP000255.1) using HISAT2 (Galaxy Version 2.2.1+galaxy1)[103]. The number of reads mapped to the

annotated genome (GCA_000013465, GFF3, EnsemblBacteria) was counted using featureCounts (Galaxy Version 2.0.8+galaxy0)[104]. MultiQC (Galaxy Version 1.27+galaxy0) was used to calculate the percentage of assigned reads[105].

Analysis of differentially expressed genes was performed using the DESeq2 package (Galaxy Version 2.11.40.8+galaxy0)[106]. Fold changes with a $P_{adj} < 0.05$ (Benjamini and Hochberg False Discovery Rate) were significant. The Volcano plot was generated using R (R version 4.4.2) and R Studio (Version 2024.12.1 + 563). Differentially expressed genes with $\log_2$fold change ≥2 in either direction were coloured orange (upregulated) and blue (downregulated). The Venn diagrams compare GGA-treated JE2 *S. aureus* cells with JE2-*saeS*::Tn mutant across three timepoints (OD_{600nm} = 0.3, 0.6 and 1.0). Gene lists were compiled by excluding genes that did not meet the following criteria: $\log_2(FC) \geq 1$ or $\log_2(FC) \leq -1$, *P-adj* < 0.05.

Gene enrichment (GO) analysis was performed for differentially expressed genes (log2(FC) ≥ 1 or log2(FC) ≤−1, P-adj<0.05), which translates to a 2-fold difference in fold change in either direction. Differentially expressed genes across all three timepoints OD_{600nm} = 0.3, 0.6 and 1.0 were pooled and analyzed. Upregulated and downregulated genes were graphed separately. Gene names were converted to STRING IDs (version 11.5) and mapped to GO pathways: Biological processes. Gene ratios were calculated by dividing the number of genes mapped to the enriched biological process by the total number of input genes. Bubble plots were generated using ggplot2 (R version 4.5.1 and R studio version 2025.09.2 + 418). Bubbles were coloured based on false-discovery rates, which were calculated by correcting raw *P*-values with the *Benjamini-Hochberg method*.

Murine subcutaneous infection model

All animal experiments were performed in compliance with guidelines set out by the Canadian Council on Animal Care and all animal protocols (AUP #2021-090) were reviewed and approved by the University of Western Ontario Animal Use Subcommittee. For all experiments, WT Balb/c mice were procured through the University of Western Ontario Animal Care and Veterinary Services (ACVS) and sourced from Charles River Laboratories. All animals were housed in a room temperature (~22°C) climate-controlled level II barrier room within the University of Western Ontario ACVS facility. Animals were maintained in microisolator cages with constant food and water access with a 12 hr light/dark cycle. ~20 h prior to infection, the left and right flanks of eight- to ten-week-old male and female Balb/c mice were shaved and treated with a chemical depilatory agent. At this time *S. aureus* USA300 LAC was cultured overnight in TSB at 37°C with aeration. On the day of the infection, *S. aureus* was sub-cultured in 50 mL of TSB and grown to an OD_{600nm} of 0.6. The bacteria were harvested by centrifugation, washed twice with 20 mL of sterile PBS, and diluted to an OD_{600nm} of 3.2 in PBS corresponding to ~5.0 × 108 CFU/mL. Immediately before infection, 0.25 mg of GGA stored at −80 °C was reconstituted in 95% EtOH at 0.61 mg/mL and then diluted in PBS to generate a 0.061 mg/mL suspension of GGA. The GGA was then mixed 1:1 with *S. aureus* yielding bacterial suspensions at an OD_{600nm} of ~1.6 with 0.031 mg/mL GGA. Vehicle control lacking GGA was also generated and similarly mixed 1:1 with *S. aureus*. Next, 50 μL of the *S. aureus*/GGA or *S. aureus*/vehicle suspensions, containing ~2.0-4.0 ×107 bacteria, were injected subcutaneously into the right and left flank of depilated mice. At 6 h post-infection, 50 μL of freshly prepared vehicle, 0.031 mg/mL GGA without bacteria were injected subcutaneously into the flanks of infected mice.

For skin infections where GGA was administered post-infection, *S. aureus* was cultured and prepared as described above; however, the bacteria were diluted to an OD_{600nm} of ~1.6 in PBS and 50 μL of this suspension was injected subcutaneously into the left and right flank of each mouse. At 1 h post-infection, the vehicle control and GGA were prepared as described above to a concentration of 0.031 mg/mL of GGA in PBS. Next, 50 μL of this GGA suspension or vehicle were administered into each site of infection by subcutaneous injection. A second dose of freshly prepared GGA at 0.031 mg/mL or vehicle control was again administered at 7 h post-infection. This corresponded to ~ 0.067 mg/Kg of GGA administered to each flank with each injection. For all infections, the mice were monitored until 48 h post-infection at which time the animals were sacrificed by cervical dislocation after being anesthetized by inhalation of isoflurane. Next, each flank was imaged, the tissue resected, and each lesion homogenized in 3 mL of sterile 0.1% (v/v) triton x-100 in PBS. The tissue homogenates were subsequently plated on mannitol salt agar, incubated ON at 37°C and then enumerated. The area of dermonecrotic lesions was determined using Fiji[107].

GGA time-kill kinetic assays

The CLSI broth microdilution method of antimicrobial susceptibility testing was used to determine the MIC of GGA against MRSA USA300 JE2 after 18 h[108]. Plates were incubated at 37 °C with aeration at 800 rpm and a BioTek LogPhase 600 microplate reader was used to measure the OD_{600nm}. The inoculum was prepared by suspending colonies grown on TSA to an OD_{600nm} of ~0.1 in sterile 0.85% (w/v) NaCl. The bacterial suspension was further diluted 100-fold in TSB. 50 μL of the 100-fold diluted cells were applied to round-bottom 96-well microtiter plates (VWR) along with 50 μL of GGA serially diluted 2-fold in TSB. A vehicle control (5% ethanol) was included. To further investigate the antibacterial activity of GGA, time-kill kinetic assays were performed in biological triplicate. Saturated overnight cultures were diluted to a starting inoculum of 1×10^5 CFU/mL in TSB or sterile PBS. GGA was profiled at different concentrations (0, 10, 50, and 100 μM), and a 0.5% ethanol vehicle control was also included. For the experiments conducted in TSB, the cultures were incubated at 37 °C with aeration at 220 rpm. For PBS, the cultures were maintained in a static state and incubated at 37 °C. The treated cultures were sampled at different time points (t = 15 min, 1 h, 8 h, and 24 h) and diluted 10-fold in sterile PBS. Ten microliters of each dilution were spotted onto TSA in a rectangular single-well plate in triplicate (Nunc OmniTray) and incubated at 37 °C for 18 h. The colonies were manually enumerated to calculate the CFU/mL at each time point.

Statistics and reproducibility

All statistical tests were performed using Graphpad 10.5.0 for macOS unless otherwise stated. The % adhesion after fatty acid treatment relative to the untreated wild-type control was compared using a two-tailed, one-sample *t*-test. Adhesion assay data and surface adhesin abundance after GGA treatment were analyzed with one-way ANOVA plus Dunnett's post-hoc test. The HMEC-1 endothelial adhesion results were compared using Brown–Forsythe/ Welch's ANOVA followed by Dunnett's T3 multiple-comparison test. Differences in fibronectin adhesion probability assessed using AFM was compared using a one-way Brown-Forsythe and Welch ANOVA test with Dunnett T3 multiple comparisons test. Immunoblots of surface adhesins were compared using a two-tailed, one sample *t*-test with Bonferroni correction for multiple comparisons. Quantification of Pro-Geh among groups were compared using a one-way ANOVA followed by Dunnett's multiple comparisons test. Fatty acid kinase complex activity in the presence of fatty acids was compared using a one-way ANOVA followed by Dunnett's multiple comparisons test. Lipid profiles before and after adding GGA was compared using multiple unpaired *t*-tests with Holm-Šidák correction. Comparisons of the surface abundance of adhesins in the *saeS*::Tn mutant were performed using a one-way ANOVA with Tukey's multiple comparisons test. Reporter activity from P*coa-lacZ* in the presence of fatty acids were compared using a one-way ANOVA with Dunnet's multiple comparisons test. Differentially expressed genes in response to GGA treatment or *saeS* disruption were analyzed using DESeq2 (Galaxy Version 2.11.40.8+galaxy0) accessed via usegalaxy.org.

Enriched Gene Ontology (GO) biological processes were identified using a one-sided Fisher's exact test after Benjamini-Hochberg correction. Finally, data corresponding to mice studies were compared using a two-tailed, unpaired *t*-test with Welch's correction.

Reporting summary

Further information on research design is available in the Nature Portfolio Reporting Summary linked to this article.

Data availability

RNA-seq data and analyses were deposited in the NCBI Gene Expression Omnibus (GEO) database under accession number GSE290916. Lipidomics method reporting is available at https://doi.org/10.5281/zenodo.18974156. Lipidomics raw data, analyzed data, and metadata have been deposited in the NIH Common Fund's National Metabolomics Data Repository (NMDR) website and the Metabolomics Workbench[109] (https://www.metabolomicsworkbench.org), where they have been assigned Study ID ST004682. The data can be accessed directly via its Project https://doi.org/10.21228/M8DP1W. This work is supported by NIH grant U2C-DK119886 and OT2-OD030544 grants. All study data are included in the article, Supplementary Data files, and/or the supplementary information. Source data are provided with this study. Source data are provided with this paper.

References

1. Naghavi, M. et al. Global burden of bacterial antimicrobial resistance 1990–2021: a systematic analysis with forecasts to 2050. Lancet *0*. https://doi.org/10.1016/s0140-6736(24)01867-1 (2024).
2. Wertheim, H. F. L. et al. The role of nasal carriage in *Staphylococcus aureus* infections. *Lancet Infect. Dis.* **5**, 751–762 (2005).
3. Leonard, A. C., Petrie, L. E. & Cox, G. Bacterial anti-adhesives: inhibition of *Staphylococcus aureus* Nasal Colonization. *ACS Infect. Dis.* **5**, 1668–1681 (2019).
4. O'Brien, L. M., Walsh, E. J., Massey, R. C., Peacock, S. J. & Foster, T. J. *Staphylococcus aureus* clumping factor B (ClfB) promotes adherence to human type I cytokeratin 10: implications for nasal colonization. *Cell. Microbiol.* **4**, 759–770 (2002).
5. Walsh, E., O'Brien, L., Liang, X., Hook, M. & Foster, T. J. Clumping Factor B, a Fibrinogen-binding MSCRAMM (Microbial Surface Components Recognizing Adhesive Matrix Molecules) Adhesin of Staphylococcus aureus, Also Binds to the Tail Region of Type I Cytokeratin 10. *J. Biol. Chem.* **279**, 50691–50699 (2004).
6. Mulcahy, M. E. et al. Nasal colonisation by *Staphylococcus aureus* depends upon clumping factor B binding to the squamous epithelial cell envelope protein loricrin. *PLoS Pathog.* **8**, e1003092 (2012).
7. Berry, K. A., Verhoef, M. T. A., Leonard, A. C. & Cox, G. *Staphylococcus aureus* adhesion to the host. *Ann. N. Y. Acad. Sci.* https://doi.org/10.1111/nyas.14807 (2022).
8. von Eiff, C., Becker, K., Machka, K., Stammer, H. & Peters, G. Nasal carriage as a source of *Staphylococcus aureus* Bacteremia. *N. Engl. J. Med.* **344**, 11–16 (2001).
9. Wertheim, H. F. L. et al. Risk and outcome of nosocomial *Staphylococcus aureus* bacteraemia in nasal carriers versus non-carriers. *Lancet* **364**, 703–705 (2004).
10. Septimus, E. J. & Schweizer, M. L. Decolonization in prevention of health care-associated infections. *Clin. Microbiol. Rev.* **29**, 201–222 (2016).
11. Poovelikunnel, T., Gethin, G. & Humphreys, H. Mupirocin resistance: clinical implications and potential alternatives for the eradication of MRSA. *J. Antimicrob. Chemother.* **70**, 2681–2692 (2015).
12. Leonard, A. C. et al. Autolysin-mediated peptidoglycan hydrolysis is required for the surface display of *Staphylococcus aureus* cell wall-anchored proteins. *Proc. Natl. Acad. Sci. USA* **120**, e2301414120 (2023).
13. Petrie, L. E., Leonard, A. C., Murphy, J. & Cox, G. Development and validation of a high-throughput whole-cell assay to investigate *Staphylococcus aureus* adhesion to host ligands. *J. Biol. Chem.* **295**, 16700–16712 (2020).
14. Mazmanian, S. K., Ton-That, H. & Schneewind, O. Sortase-catalysed anchoring of surface proteins to the cell wall of *Staphylococcus aureus*. *Mol. Microbiol.* **40**, 1049–1057 (2001).
15. Matano, L. M., Morris, H. G., Wood, B. M., Meredith, T. C. & Walker, S. Accelerating the discovery of antibacterial compounds using pathway-directed whole cell screening. *Bioorg. Med. Chem.* **24**, 6307–6314 (2016).
16. Payne, D. J., Gwynn, M. N., Holmes, D. J. & Pompliano, D. L. Drugs for bad bugs: confronting the challenges of antibacterial discovery. *Nat. Rev. Drug Discov.* **6**, 29–40 (2007).
17. Tenover, F. C. & Goering, R. V. Methicillin-resistant *Staphylococcus aureus* strain USA300: origin and epidemiology. *J. Antimicrob. Chemother.* **64**, 441–446 (2009).
18. Diekema, D. J. et al. Continued emergence of USA300 methicillin-resistant *Staphylococcus aureus* in the United States: results from a nationwide surveillance study. *Infect. Control Hosp. Epidemiol.* **35**, 285–292 (2014).
19. Al-Rawahi, G. N. et al. Community-associated CMRSA-10 (USA-300) is the predominant strain among methicillin-resistant Staphylococcus aureus strains causing skin and soft tissue infections in patients presenting to the emergency department of a Canadian tertiary care hospital. *J. Emerg. Med.* **38**, 6–11 (2010).
20. Mangat, C. S., Bharat, A., Gehrke, S. S. & Brown, E. D. Rank ordering plate data facilitates data visualization and normalization in high-throughput screening. *J. Biomol. Screen.* **19**, 1314–1320 (2014).
21. Shidoji, Y. & Ogawa, H. Natural occurrence of cancer-preventive geranylgeranoic acid in medicinal herbs. *J. Lipid Res.* **45**, 1092–1103 (2004).
22. Sakane, C., Okitsu, T., Wada, A., Sagami, H. & Shidoji, Y. Inhibition of lysine-specific demethylase 1 by the acyclic diterpenoid geranylgeranoic acid and its derivatives. *Biochem. Biophys. Res. Commun.* **444**, 24–29 (2014).
23. Kim, S.-H. & Oh, K.-B. Evaluation of antimicrobial activity of farnesoic acid derivatives. *J. Microbiol. Biotechnol.* **12**, 1006–1009 (2002).
24. Stenz, L. et al. Impact of oleic acid (cis-9-octadecenoic acid) on bacterial viability and biofilm production in *Staphylococcus aureus*. *FEMS Microbiol. Lett.* **287**, 149–155 (2008).
25. Kim, Y.-G. et al. Herring oil and omega fatty acids inhibit *Staphylococcus aureus* biofilm formation and virulence. *Front. Microbiol.* **9**, 1241 (2018).
26. Lee, J.-H., Kim, Y.-G. & Lee, J. Inhibition of *Staphylococcus aureus* biofilm formation and virulence factor production by petroselinic acid and other unsaturated C18 fatty acids. *Microbiol. Spectr.* **10**, e0133022 (2022).
27. Sinha, B. et al. Fibronectin-binding protein acts as *Staphylococcus aureus* invasin via fibronectin bridging to integrin alpha5beta1. *Cell. Microbiol.* **1**, 101–117 (1999).
28. Dziewanowska, K. et al. Fibronectin binding protein and host cell tyrosine kinase are required for internalization of *Staphylococcus aureus* by epithelial cells. *Infect. Immun.* **67**, 4673–4678 (1999).
29. Josse, J., Laurent, F. & Diot, A. Staphylococcal adhesion and host cell invasion: fibronectin-binding and other mechanisms. *Front. Microbiol.* **8**, 2433 (2017).
30. Tran Van Nhieu, G. & Isberg, R. R. Bacterial internalization mediated by beta 1 chain integrins is determined by ligand affinity and receptor density. *EMBO J.* **12**, 1887–1895 (1993).

31. Fowler, T. et al. Cellular invasion by *Staphylococcus aureus* involves a fibronectin bridge between the bacterial fibronectin-binding MSCRAMMs and host cell beta1 integrins. *Eur. J. Cell Biol.* **79**, 672–679 (2000).
32. Mazmanian, S. K., Liu, G., Jensen, E. R., Lenoy, E. & Schneewind, O. *Staphylococcus aureus* sortase mutants defective in the display of surface proteins and in the pathogenesis of animal infections. *Proc. Natl. Acad. Sci. USA* **97**, 5510–5515 (2000).
33. Mazmanian, S. K., Liu, G., Ton-That, H. & Schneewind, O. *Staphylococcus aureus* sortase, an enzyme that anchors surface proteins to the cell wall. *Science* **285**, 760–763 (1999).
34. Goncheva, M. I., Gibson, R. M., Shouldice, A. C., Dikeakos, J. D. & Heinrichs, D. E. The *Staphylococcus aureus* protein IsdA increases SARS CoV-2 replication by modulating JAK-STAT signaling. *iScience* **26**, 105975 (2023).
35. Atkins, K. L. et al. *S. aureus* IgG-binding proteins SpA and Sbi: host specificity and mechanisms of immune complex formation. *Mol. Immunol.* **45**, 1600–1611 (2008).
36. Clarke, S. R., Wiltshire, M. D. & Foster, S. J. IsdA of *Staphylococcus aureus* is a broad spectrum, iron-regulated adhesin. *Mol. Microbiol.* **51**, 1509–1519 (2004).
37. Buck, A. W. et al. Bonds between fibronectin and fibronectin-binding proteins on *Staphylococcus aureus* and *Lactococcus lactis*. *Langmuir* **26**, 10764–10770 (2010).
38. Herman-Bausier, P., El-Kirat-Chatel, S., Foster, T. J., Geoghegan, J. A. & Dufrêne, Y. F. *Staphylococcus aureus* fibronectin-binding protein A mediates cell-cell adhesion through low-affinity homophilic bonds. *MBio* **6**, e00413–e00415 (2015).
39. Viljoen, A., Mignolet, J., Viela, F., Mathelié-Guinlet, M. & Dufrêne, Y. F. How microbes use force to control adhesion. *J. Bacteriol.* **202**, e00125-20 (2020).
40. Gimza, B. D. et al. Unraveling the impact of secreted proteases on hypervirulence in *Staphylococcus aureus*. *MBio* **12**, e03288-20 (2021).
41. Arsic, B., Zhu, Y., Heinrichs, D. E. & McGavin, M. J. Induction of the staphylococcal proteolytic cascade by antimicrobial fatty acids in community acquired methicillin resistant *Staphylococcus aureus*. *PLoS One* **7**, e45952 (2012).
42. Massimi, I. et al. Identification of a novel maturation mechanism and restricted substrate specificity for the SspB cysteine protease of *Staphylococcus aureus*. *J. Biol. Chem.* **277**, 41770–41777 (2002).
43. Imamura, T. et al. Induction of vascular leakage through release of bradykinin and a novel kinin by cysteine proteinases from *Staphylococcus aureus*. *J. Exp. Med.* **201**, 1669–1676 (2005).
44. McGavin, M. J., Zahradka, C., Rice, K. & Scott, J. E. Modification of the *Staphylococcus aureus* fibronectin binding phenotype by V8 protease. *Infect. Immun.* **65**, 2621–2628 (1997).
45. Karlsson, A., Saravia-Otten, P., Tegmark, K., Morfeldt, E. & Arvidson, S. Decreased amounts of cell wall-associated protein A and fibronectin-binding proteins in *Staphylococcus aureus sarA* mutants due to up-regulation of extracellular proteases. *Infect. Immun.* **69**, 4742–4748 (2001).
46. McAleese, F. M., Walsh, E. J., Sieprawska, M., Potempa, J. & Foster, T. J. Loss of clumping factor B fibrinogen binding activity by *Staphylococcus aureus* involves cessation of transcription, shedding and cleavage by metalloprotease. *J. Biol. Chem.* **276**, 29969–29978 (2001).
47. Ohbayashi, T. et al. Degradation of fibrinogen and collagen by staphopains, cysteine proteases released from *Staphylococcus aureus*. *Microbiology* **157**, 786–792 (2011).
48. Subramanian, C., Frank, M. W., Yun, M.-K. & Rock, C. O. The Phospholipase A1 Activity of Glycerol Ester Hydrolase (Geh) Is Responsible for Extracellular 2-12(S)-Methyltetradecanoyl-Lysophosphatidylglycerol Production in *Staphylococcus aureus*. *mSphere* **8**, e0003123 (2023).
49. Busche, T. et al. Comparative secretome analyses of human and zoonotic *Staphylococcus aureus* Isolates CC8, CC22, and CC398. *Mol. Cell. Proteom.* **17**, 2412–2433 (2018).
50. Parsons, J. B. et al. Identification of a two-component fatty acid kinase responsible for host fatty acid incorporation by *Staphylococcus aureus*. *Proc. Natl. Acad. Sci. USA* **111**, 10532–10537 (2014).
51. Parsons, J. B., Frank, M. W., Jackson, P., Subramanian, C. & Rock, C. O. Incorporation of extracellular fatty acids by a fatty acid kinase-dependent pathway in *Staphylococcus aureus*. *Mol. Microbiol.* **92**, 234–245 (2014).
52. DeMars, Z., Singh, V. K. & Bose, J. L. Exogenous Fatty Acids Remodel *Staphylococcus aureus* Lipid Composition through Fatty Acid Kinase. *J. Bacteriol.* **202**, e00128-20 (2020).
53. Kuiack, R. C. et al. The *fadXDEBA* locus of *Staphylococcus aureus* is required for metabolism of exogenous palmitic acid and in vivo growth. *Mol. Microbiol.* **120**, 425–438 (2023).
54. Myers, M. J. et al. Molecular insights into the structure and function of the *Staphylococcus aureus* fatty acid kinase. *J. Biol. Chem.* **300**, 107920 (2024).
55. Neumann, Y. et al. The effect of skin fatty acids on *Staphylococcus aureus*. *Arch. Microbiol.* **197**, 245–267 (2015).
56. Ericson, M. E., Subramanian, C., Frank, M. W. & Rock, C. O. Role of Fatty Acid Kinase in Cellular Lipid Homeostasis and SaeRS-Dependent Virulence Factor Expression in *Staphylococcus aureus*. *MBio* **8**, e00988-17 (2017).
57. Krute, C. N., Rice, K. C. & Bose, J. L. VfrB Is a Key Activator of the *Staphylococcus aureus* SaeRS Two-Component System. *J. Bacteriol.* **199**, e00828-16 (2017).
58. Bose, J. L., Daly, S. M., Hall, P. R. & Bayles, K. W. Identification of the *Staphylococcus aureus vfrAB* operon, a novel virulence factor regulatory locus. *Infect. Immun.* **82**, 1813–1822 (2014).
59. DeMars, Z. R. et al. Fatty acids can inhibit *Staphylococcus aureus* SaeS activity at the membrane independent of alterations in respiration. *Mol. Microbiol.* **116**, 1378–1391 (2021).
60. Nygaard, T. K. et al. SaeR binds a consensus sequence within virulence gene promoters to advance USA300 pathogenesis. *J. Infect. Dis.* **201**, 241–254 (2010).
61. Corrigan, R. M. & Foster, T. J. An improved tetracycline-inducible expression vector for *Staphylococcus aureus*. *Plasmid* **61**, 126–129 (2009).
62. Bateman, B. T., Donegan, N. P., Jarry, T. M., Palma, M. & Cheung, A. L. Evaluation of a tetracycline-inducible promoter in *Staphylococcus aureus* in vitro and in vivo and its application in demonstrating the role of sigB in microcolony formation. *Infect. Immun.* **69**, 7851–7857 (2001).
63. Rogasch, K. et al. Influence of the two-component system SaeRS on global gene expression in two different *Staphylococcus aureus* strains. *J. Bacteriol.* **188**, 7742–7758 (2006).
64. Lopez, M. S. et al. Host-derived fatty acids activate type VII secretion in *Staphylococcus aureus*. *Proc. Natl. Acad. Sci. USA* **114**, 11223–11228 (2017).
65. Alnaseri, H. et al. Inducible expression of a resistance-nodulation-division-type efflux pump in *Staphylococcus aureus* provides resistance to linoleic and arachidonic acids. *J. Bacteriol.* **197**, 1893–1905 (2015).
66. Shidoji, Y. Geranylgeranoic acid, a bioactive and endogenous fatty acid in mammals: a review. *J. Lipid Res.* **64**, 100396 (2023).
67. Shidoji, Y. & Tabata, Y. Unequivocal evidence for endogenous geranylgeranoic acid biosynthesized from mevalonate in mammalian cells. *J. Lipid Res.* **60**, 579–593 (2019).
68. Muto, Y. et al. Prevention of second primary tumors by an acyclic retinoid, polyprenoic acid, in patients with hepatocellular carcinoma. Hepatoma Prevention Study Group. *N. Engl. J. Med.* **334**, 1561–1567 (1996).

69. Muto, Y., Moriwaki, H. & Omori, M. In vitro binding affinity of novel synthetic polyprenoids (polyprenoic acids) to cellular retinoid-binding proteins. *Gan* **72**, 974–977 (1981).
70. Araki, H., Shidoji, Y., Yamada, Y., Moriwaki, H. & Muto, Y. Retinoid agonist activities of synthetic geranyl geranoic acid derivatives. *Biochem. Biophys. Res. Commun.* **209**, 66–72 (1995).
71. Muto, Y., Moriwaki, H. & Saito, A. Prevention of second primary tumors by an acyclic retinoid in patients with hepatocellular carcinoma. *N. Engl. J. Med.* **340**, 1046–1047 (1999).
72. Alexander, E. H. & Hudson, M. C. Factors influencing the internalization of *Staphylococcus aureus* and impacts on the course of infections in humans. *Appl. Microbiol. Biotechnol.* **56**, 361–366 (2001).
73. Rezzoagli, C., Archetti, M., Mignot, I., Baumgartner, M. & Kümmerli, R. Combining antibiotics with antivirulence compounds can have synergistic effects and reverse selection for antibiotic resistance in *Pseudomonas aeruginosa*. *PLoS Biol.* **18**, e3000805 (2020).
74. England, R. J., Homer, J. J., Knight, L. C. & Ell, S. R. Nasal pH measurement: a reliable and repeatable parameter. *Clin. Otolaryngol. Allied Sci.* **24**, 67–68 (1999).
75. Atherton, J. C. Acid–base balance: maintenance of plasma pH. *Anaesth. Intensive Care Med.* **10**, 557–561 (2009).
76. Wallace, L. A., Gwynne, L. & Jenkins, T. Challenges and opportunities of pH in chronic wounds. *Ther. Deliv.* **10**, 719–735 (2019).
77. Massey, R. C. et al. Fibronectin-binding protein A of *Staphylococcus aureus* has multiple, substituting, binding regions that mediate adherence to fibronectin and invasion of endothelial cells. *Cell. Microbiol.* **3**, 839–851 (2001).
78. Liu, Q., Yeo, W.-S. & Bae, T. The SaeRS two-component system of *Staphylococcus aureus*. *Genes* **7**, 81 (2016).
79. Kennedy, A. D. et al. Targeting of alpha-hemolysin by active or passive immunization decreases severity of USA300 skin infection in a mouse model. *J. Infect. Dis.* **202**, 1050–1058 (2010).
80. Xiong, Y. Q., Willard, J., Yeaman, M. R., Cheung, A. L. & Bayer, A. S. Regulation of *Staphylococcus aureus* alpha-toxin gene (*hla*) expression by agr, sarA, and sae in vitro and in experimental infective endocarditis. *J. Infect. Dis.* **194**, 1267–1275 (2006).
81. Marchand, V. Trans fats: What physicians should know. *Paediatr. Child Health* **15**, 373–378 (2010).
82. Mascher, T. Bacterial (intramembrane-sensing) histidine kinases: signal transfer rather than stimulus perception. *Trends Microbiol.* **22**, 559–565 (2014).
83. Adhikari, R. P. & Novick, R. P. Regulatory organization of the staphylococcal *sae* locus. *Microbiology* **154**, 949–959 (2008).
84. Liu, Q., Cho, H., Yeo, W.-S. & Bae, T. The extracytoplasmic linker peptide of the sensor protein SaeS tunes the kinase activity required for staphylococcal virulence in response to host signals. *PLoS Pathog.* **11**, e1004799 (2015).
85. Jeong, D.-W. et al. The auxiliary protein complex SaePQ activates the phosphatase activity of sensor kinase SaeS in the SaeRS two-component system of *Staphylococcus aureus*. *Mol. Microbiol.* **86**, 331–348 (2012).
86. Cao, K. et al. Fatty acid profiling in facial sebum and erythrocytes from adult patients with moderate acne. *Front. Physiol.* **13**, 921866 (2022).
87. Quehenberger, O. et al. Lipidomics reveals a remarkable diversity of lipids in human plasma. *J. Lipid Res.* **51**, 3299–3305 (2010).
88. Huber, A. H. & Kleinfeld, A. M. Unbound free fatty acid profiles in human plasma and the unexpected absence of unbound palmitoleate. *J. Lipid Res.* **58**, 578–585 (2017).
89. Picardo, M., Ottaviani, M., Camera, E. & Mastrofrancesco, A. Sebaceous gland lipids. *Dermatoendocrinol* **1**, 68–71 (2009).
90. Quehenberger, O. & Dennis, E. A. The human plasma lipidome. *N. Engl. J. Med.* **365**, 1812–1823 (2011).
91. Nguyen, M. T., Hanzelmann, D., Härtner, T., Peschel, A. & Götz, F. Skin-specific unsaturated fatty acids boost the *Staphylococcus aureus* innate immune response. *Infect. Immun.* **84**, 205–215 (2016).
92. Parsons, J. B., Yao, J., Frank, M. W., Jackson, P. & Rock, C. O. Membrane disruption by antimicrobial fatty acids releases low-molecular-weight proteins from *Staphylococcus aureus*. *J. Bacteriol.* **194**, 5294–5304 (2012).
93. Ruzin, A. & Novick, R. P. Equivalence of lauric acid and glycerol monolaurate as inhibitors of signal transduction in *Staphylococcus aureus*. *J. Bacteriol.* **182**, 2668–2671 (2000).
94. Bose, J. L., Fey, P. D. & Bayles, K. W. Genetic tools to enhance the study of gene function and regulation in *Staphylococcus aureus*. *Appl. Environ. Microbiol.* **79**, 2218–2224 (2013).
95. Wörmann, M. E., Reichmann, N. T., Malone, C. L., Horswill, A. R. & Gründling, A. Proteolytic cleavage inactivates the *Staphylococcus aureus* lipoteichoic acid synthase. *J. Bacteriol.* **193**, 5279–5291 (2011).
96. Bose, J. L., Lehman, M. K., Fey, P. D. & Bayles, K. W. Contribution of the *Staphylococcus aureus* Atl AM and GL murein hydrolase activities in cell division, autolysis, and biofilm formation. *PLoS One* **7**, e42244 (2012).
97. Sader, J. E., Larson, I., Mulvaney, P. & White, L. R. Method for the calibration of atomic force microscope cantilevers. *Rev. Sci. Instrum.* **66**, 3789–3798 (1995).
98. Odijk, T. Stiff chains and filaments under tension. *Macromolecules* **28**, 7016–7018 (1995).
99. Krute, C. N., Seawell, N. A. & Bose, J. L. Measuring staphylococcal promoter activities using a codon-optimized β-galactosidase reporter. *Methods Mol. Biol.* **2341**, 37–44 (2021).
100. Berry, K. A. et al. The *Staphylococcus aureus* esterase FmtA is essential for wall teichoic acid D-alanylation. *MBio* **16**, e0233725 (2025).
101. Bustin, S. A. et al. The MIQE guidelines: minimum information for publication of quantitative real-time PCR experiments. *Clin. Chem.* **55**, 611–622 (2009).
102. Jawaharraj, K., Peta, V., Dhiman, S. S., Gnimpieba, E. Z. & Gadhamshetty, V. Transcriptome-wide marker gene expression analysis of stress-responsive sulfate-reducing bacteria. *Sci. Rep.* **13**, 16181 (2023).
103. Kim, D., Langmead, B. & Salzberg, S. L. HISAT: a fast spliced aligner with low memory requirements. *Nat. Methods* **12**, 357–360 (2015).
104. Liao, Y., Smyth, G. K. & Shi, W. featureCounts: an efficient general purpose program for assigning sequence reads to genomic features. *Bioinformatics* **30**, 923–930 (2014).
105. Ewels, P., Magnusson, M., Lundin, S. & Käller, M. MultiQC: summarize analysis results for multiple tools and samples in a single report. *Bioinformatics* **32**, 3047–3048 (2016).
106. Love, M. I., Huber, W. & Anders, S. Moderated estimation of fold change and dispersion for RNA-seq data with DESeq2. *Genome Biol.* **15**, 550 (2014).
107. Schindelin, J. et al. Fiji: an open-source platform for biological-image analysis. *Nat. Methods* **9**, 676–682 (2012).
108. Patel J. B. et al. WPMZLB M07-A10: Methods for Dilution Antimicrobial Susceptibility Tests for Bacteria That Grow Aerobically; Approved Standard—Tenth Edition. CLSI (Clinical Lab Stand Institute) (2015).
109. Metabolomics Workbench: An international repository for metabolomics data and metadata, metabolite standards, protocols, tutorials and training, and analysis tools (2016)'. [PubMed: https://www.ncbi.nlm.nih.gov/pubmed/26467476/].

Acknowledgements

We would like to acknowledge the Centre for Microbial Cell Biology at McMaster University, especially Dr. Tracey Campbell, Cecilia Murphy, and Susan McCusker, for their support with the technical aspects of the

chemical screen. We thank Dr. Gerry Wright at McMaster University for generously providing access to his clinical isolate collection, and Mr. David W. Watson at Western University for assistance with training and optimization of the endothelial cell adhesion assay. The lipid analysis described in this work was performed at the Kansas Lipidomics Research Center Analytical Laboratory. Instrument acquisition and lipidomic method development were supported by the National Science Foundation (EPS 0236913, MCB 1413036, MCB 0920663, DBI 0521587, DBI1228622), Kansas Technology Enterprise Corporation, K-IDeA Networks of Biomedical Research Excellence (INBRE) of the National Institute of Health (P20GM103418), and Kansas State University. SeqCenter (Pittsburgh, PA) and the Advanced Analysis Centre at the University of Guelph (Ontario, Canada) performed the RNA sequencing. This study was funded by a Canadian Institutes of Health Research grant (PJT-436506) and a Tier 2 Canada Research Chair award awarded to G.C. This study was also supported by funds from the Canadian Foundation for Innovation (JELF 37730 and 43704) to G.C. and a Doctoral Research Award awarded to A.C.L. through the Canada Graduate Scholarships program. Work at the Université catholique de Louvain was supported by the National Fund for Scientific Research (FNRS). Y.F.D. is a Research Director at the FNRS. Work at the University of Western Ontario was supported by a CIHR grant PJT-197907 awarded to D.E.H. Work at the University of Nebraska Medical Center was supported by NIAID grant AI153773. Work at the University of Kansas Medical Center was supported by NIAID grant AI186276 to J.L.B.

Author contributions

G.C., D.E.H., J.L.B., and Y.D. designed the research; A.C.L. and R.B. performed the research and analysed the data, except where noted. Z.Z. and T.O.P. performed the AFM experiments; Z.Z., T.O.P., and Y.D. analyzed the AFM data. C.M. and M.J.M. performed the Fak enzyme assay and the *sae* reporter assay, and C.M., M.J.M., and J.L.B. analysed the data. K.A.B. performed the SEM and analyzed the data. K.W.B. and J.L.B. constructed the protease-deficient mutant. R.S.F. performed the endothelial cell adhesion assays and analyzed the data. R.S.F. and D.E.H completed the animal work and analyzed the data. G.C., A.C.L., and R.B. wrote the paper, and all authors read the manuscript and provided comments.

Competing interests

The authors declare no competing interests.

Additional information

Supplementary information The online version contains supplementary material available at (https://doi.org/10.1038/s41467-026-71917-8).

Correspondence and requests for materials should be addressed to Georgina Cox.

Peer review information *Nature Communications* thanks the anonymous reviewers for their contribution to the peer review of this work. A peer review file is available.